Geochimica et Cosmochimica Acta 375 (2024) 36–49

Contents lists available at ScienceDirect

Geochimica et Cosmochimica Acta

journal homepage: www.elsevier.com/locate/gca

# Alumina solubility in periclase determined to lower mantle conditions and implications for ferropericlase inclusions in diamonds

Lianjie Man [a,*], Hongzhan Fei [a,b], Eun Jeong Kim [a], Adrien Néri [a], Longjian Xie [a,c], Daniel J. Frost [a]

[a] Bayerisches Geoinstitut, Universität Bayreuth, Bayreuth, Germany
[b] Key Laboratory of Geoscience Big Data and Deep Resource of Zhejiang Province, School of Earth Sciences, Zhejiang University, Hangzhou, China
[c] Department of Earth Sciences, University College London, London WC1E6BS, UK

ARTICLE INFO

*Associate editor*: James Van Orman

*Keywords:*
Periclase alumina solubility
Lower mantle
Diamond inclusions
Mantle temperature

ABSTRACT

A series of high-pressure multi-anvil experiments were conducted in the MgO-$Al_2O_3$ system between 15 and 50 GPa and at temperatures up to 2623 K, to determine the solubility of $Al_2O_3$ in periclase in the stability fields of coexisting spinel, corundum, the $Mg_2Al_2O_5$ modified ludwigite phase, the $MgAl_2O_4$ calcium ferrite phase, and the $MgAl_2O_4$ calcium titanate phase. The $Al_2O_3$ solubility in periclase is strongly temperature-dependent over the conditions investigated. Conversely, periclase $Al_2O_3$ solubility exhibits a negative relationship with pressure. Experiments with up to 40 mol.% FeO in ferropericlase show $Al_2O_3$ solubilities that are near identical to those of periclase, within experimental uncertainties. A simple thermodynamic model incorporating significant literature on ambient pressure measurements is able to describe periclase $Al_2O_3$ solubility up to 40 GPa. This model is used to investigate the $Al_2O_3$ contents of ferropericlase inclusions observed in natural diamonds, which vary up to 0.35 mol. %. Pressure–temperature curves along which particular inclusions formed can be produced if equilibrium can be assumed with Al-bearing minerals found in the same diamond. Alternatively, the maximum possible $Al_2O_3$ content in ferropericlase can be determined for a certain pressure–temperature profile and inclusions with $Al_2O_3$ contents that exceed this curve can be excluded from those conditions. To obtain such solubility curves, calculations are performed for periclase coexisting with the Al-rich phases spinel, garnet, bridgmanite and the $MgAl_2O_4$ calcium ferrite phase. The calculations indicate that periclase, and by inference ferropericlase, $Al_2O_3$-contents cannot be greater than 0.5 mol.% under present day adiabatic mantle temperatures and go through a minimum at mantle transition zone conditions. This excludes a number of Al-rich ferropericlase inclusions found in natural diamonds from being formed in the transition zone, unless temperatures were super-adiabatic. This subset of inclusions likely formed either at the base of the upper mantle or the top of the lower mantle, but must have formed at near adiabatic temperatures. The majority of ferropericlase inclusions have $Al_2O_3$ contents that would be consistent with formation in the transition zone at near slab temperatures, but could still have been formed at higher temperatures if $Al_2O_3$ activities were low.

## 1. Introduction

Determining the formation conditions of sublithospheric diamonds is important as they provide evidence for the mobility of carbon-bearing fluids or melts in the Earth's deep convecting interior (Stachel, 2001; Walter et al., 2011). The inclusions captured inside diamonds can potentially provide information on these formation conditions and possibly on the nature of the mobile carbon-bearing medium from which they formed (Anzolini et al., 2019; Thomson et al., 2016). Ferropericlase, (Mg,Fe)O, is apparently the most common type of inclusion found in proposed sublithospheric diamonds, and is often used to identify them as originating from the lower mantle (Harte, 1999; Hayman et al., 2005). Ferropericlase is, most likely, the second most abundant phase in the bulk of the lower mantle (Irifune and Tsuchiya, 2007). The high molar Fe/(Fe + Mg) ratios of some ferropericlase inclusions, which extend to values >0.8, have also been attributed to an origin in the deep lower mantle due to either a pressure dependent shift in interphase Fe-Mg partitioning, or interaction between the mantle and

* Corresponding author.
*E-mail address:* lianjie.man@uni-bayreuth.de (L. Man).

https://doi.org/10.1016/j.gca.2024.05.002
Received 1 October 2023; Accepted 4 May 2024
Available online 7 May 2024

core (Hayman et al., 2005; Kaminsky, 2012). Other studies have pointed out that ferropericlase could also form as a result of either decarbonation, or more likely reduction of carbonate melts (Liu, 2002; Brey et al., 2004; Thomson et al., 2016; Bulatov et al., 2019), at potentially any depth in the mantle. Diverse origins of ferropericlase inclusions are in fact supported by recent studies (Nimis et al., 2019; Lorenzon et al., 2023), that determined crystallographic orientation relationships (CORs) between inclusions and their diamond hosts. Specific CORs were observed only for Fe-rich ferropericlase inclusions, potentially implying a distinct syngenetic origin, versus a protogenetic origin for inclusions with lower Fe-contents that display random CORs.

By utilizing elastic geobarometry, where residual pressures are measured for inclusions still trapped in diamonds, it has been possible to determine that some ferropericlase inclusions have formation pressures ranging to at least 22.1 GPa (Anzolini et al., 2019; Nestola et al., 2023a). Such a technique provides a pressure–temperature (P-T) curve along which entrapment likely occurred (Angel et al., 2022; Kohn et al., 2023), but requires a complementary method in order to pinpoint both P and T conditions, as in traditional thermobarometry-thermometry assessments (e.g., Nimis, 2022).

In addition to FeO and MgO, there are a number of minor elements in natural ferropericlase inclusions, the concentration of which might reveal information on the formation conditions. For instance, the $Fe^{3+}/\Sigma Fe$ ratio of ferropericlase diamond inclusions has been used as an indicator of the redox conditions at which the diamonds formed (e.g., Wirth et al., 2014; Kaminsky et al., 2015; Kiseeva et al., 2022; Nestola et al., 2023b). One possibility is that the incorporation of $Al_2O_3$ into the structure of ferropericlase, which occurs via the component $(Al_{2/3},Va_{1/3})O$, where Va is a cation vacancy (Hallstedt, 1992), might reveal information on the P or T conditions of equilibrium. The effects of changing conditions on $Al_2O_3$ incorporation may also be of broader interest because $Al_2O_3$ has already been shown to have a marked effect on ferropericlase transport properties, such as electrical conductivity and diffusivity (e.g., Sempolinski and Kingery, 1980; Van Orman et al., 2003, 2009; Ammann et al., 2012; Riet et al., 2020). For example, the presence of just 0.1 mol.% $Al_2O_3$ raises the rate of Mg self-diffusion in periclase by 1–2 orders of magnitude at 25 GPa (Van Orman et al., 2003).

Ferropericlase inclusions found in natural diamonds have $Al_2O_3$ concentrations that range up to 0.35 mol. %, although the majority of samples have concentrations that are an order of magnitude lower than this (Walter et al., 2022). The variability in the $Al_2O_3$ concentration may provide information on the P, T, or $Al_2O_3$ activity at which the inclusions formed. Although it is difficult to independently assess the $Al_2O_3$ activity during formation, a maximum limit can be determined by assuming saturation with a mantle $Al_2O_3$-bearing phase, such as spinel or garnet. Knowledge of the P-T dependency of ferropericlase $Al_2O_3$ solubility should allow formation conditions to be excluded under which particular ferropericlase inclusions would have $Al_2O_3$ concentrations that exceed this upper limit. Alternatively, it may be possible to independently determine $Al_2O_3$ activity from the presence of proposed co-forming phases, such as garnet, in the same growth zone of the diamond.

Phase relations in the MgO-$Al_2O_3$ system have been intensively studied at ambient pressure under varying temperatures (e.g., Alper et al., 1962; Stubican and Roy, 1965; Mori, 1982; Zienert and Fabrichnaya, 2013). Periclase forms a limited solid solution with $Al_2O_3$, which is T dependent. At saturation with coexisting $MgAl_2O_4$ spinel, the periclase $Al_2O_3$ content reaches a value of approximately 9 mol % at 2500 K (Zienert and Fabrichnaya, 2013). However, currently the mixing behaviour of MgO and $Al_2O_3$ in periclase remains unexplored at high P and T. In addition to spinel, a series of $Al_2O_3$-rich phases which can coexist with periclase have been identified in the MgO-$Al_2O_3$ system under high P and T conditions, including $Al_2O_3$ corundum (Liu, 1975; Akaogi et al., 1999; Irifune et al., 2002; Kojitani et al., 2010), a calcium ferrite-structured $MgAl_2O_4$ (CF) phase (Irifune et al., 1991; Akaogi et al., 1999; Irifune et al., 2002), an $Mg_2Al_2O_5$ phase with a modified ludwigite (Ldw) structure (Enomoto et al., 2009; Kojitani et al., 2010), and an $MgAl_2O_4$ calcium titanite (CT) phase (Ono et al., 2005, 2006). The formation of various high-pressure $Al_2O_3$-rich phases will alter the $Al_2O_3$ activity within the system adding further complexity to the experimental study of the solubility behaviour.

In this study, we have performed a series of high-P and high-T multi-anvil experiments within the MgO-$Al_2O_3$ system, reaching pressures up to 50 GPa, to investigate the solubility of $Al_2O_3$ in periclase to lower mantle conditions. Complementary experiments were conducted in the FeO-MgO-$Al_2O_3$ system at 21 GPa and up to 2300 K to evaluate the potential influence of FeO on the solubility of $Al_2O_3$ in natural ferropericlase. Based on the experimental results, we evaluate the factors affecting the $Al_2O_3$ concentration in ferropericlase in the sublithospheric mantle and discuss the P-T formation conditions of ferropericlase inclusions found in natural diamonds.

## 2. Materials and methods

For experiments conducted in the MgO-$Al_2O_3$ system, mixtures of reagent-grade MgO and $Al_2O_3$ powders with grain sizes of ~1 μm were used as starting materials. Powders with MgO:$Al_2O_3$ molar ratios of 6:1 and 12:1 were ground with ethanol in an agate mortar for around 1 h to ensure the mixtures were homogenous. The mixtures were then dried overnight and stored in an oven at 125 °C before being loaded into high-pressure multi-anvil assemblies. For complementary experiments investigating the effect of FeO on the $Al_2O_3$ solubility in ferropericlase, (Mg,Fe)O pellets containing 20 mol.% (Fp80) and 40 mol.% (Fp60) FeO were synthesized from dried mixtures of reagent-grade $Fe_2O_3$ and MgO in a CO-$CO_2$ gas mixing furnace at 1100 °C and an oxygen fugacity two log units below the fayalite-magnetite-quartz oxygen buffer. The recovered Fp80 and Fp60 pellets were ground and then mixed with $Al_2O_3$ in a molar ratio of 6:1. An Fp90 composition was produced from powders of Fp80 and MgO, and also mixed 6:1 with $Al_2O_3$. Approximately 5 wt% metallic iron with a grain size <10 μm was mixed with the resulting starting materials to control the oxygen fugacity.

We used multi-anvil presses with either a split-sphere guide block (Hymag) or an Osugi-type guide block (IRIS-15) at the Bayerisches Geoinstitut (BGI), for experiments between 15–23 GPa and 27–50 GPa, respectively. The methodologies and pressure calibrations for the Hymag press are described by Keppler and Frost (2005), and by Ishii et al. (2016) for the IRIS-15. A $Cr_2O_3$-doped MgO octahedron with a 10 mm edge length (OEL = 10 mm) was used with eight tungsten carbide cubic anvils with 4 mm truncation edge lengths (TEL = 4 mm, Ha06 cubes from Hawedia) for experiments between 15 and 23 GPa and cell assemblies with OEL/TEL = 7 mm/3 mm and 5.7 mm/1.5 mm (F05 cubes from Fuji Die Co. Ltd.) for experiments at 27 GPa and 33 GPa, respectively. For an experiment at 50 GPa, a 5.7 mm/1.5 mm cell assembly was used with eight ultrahard 1°-tapered TJS01 tungsten carbide anvils (Fuji Die Co. Ltd), as calibrated by Ishii et al., 2019.

In each experiment in the MgO-$Al_2O_3$ system, except runs I1193 and H5299, the starting material was placed as a thin layer (≤100 μm) next to the hot junction of a type-D thermocouple (TC), to minimize the differences between TC readings and the sample temperatures, given the large temperature gradients in the higher pressure assemblies (e.g., van Westrenen et al., 2003). No correction was applied to the thermocouple emf to account for a possible pressure effect. Another sample capsule was usually placed adjacent to the MgO-$Al_2O_3$ mixture for a separate purpose, unrelated to the current study. As shown in Fig. 1a, the materials surrounding the MgO-$Al_2O_3$ samples were the MgO and $Al_2O_3$ ceramic components of the high-P assembly, which do not, therefore, introduce contamination into the samples. For run I1193, the TC was directly in contact with the centre of the rhenium furnace, and the temperature reading is therefore the temperature of the furnace. In run H5299, a semi-sintered MgO tube with 1.8 mm outer diameter and 1.2 mm inner diameter was filled with the sample and then placed into the cylindrical $LaCrO_3$ furnace. In this case only the sample composition

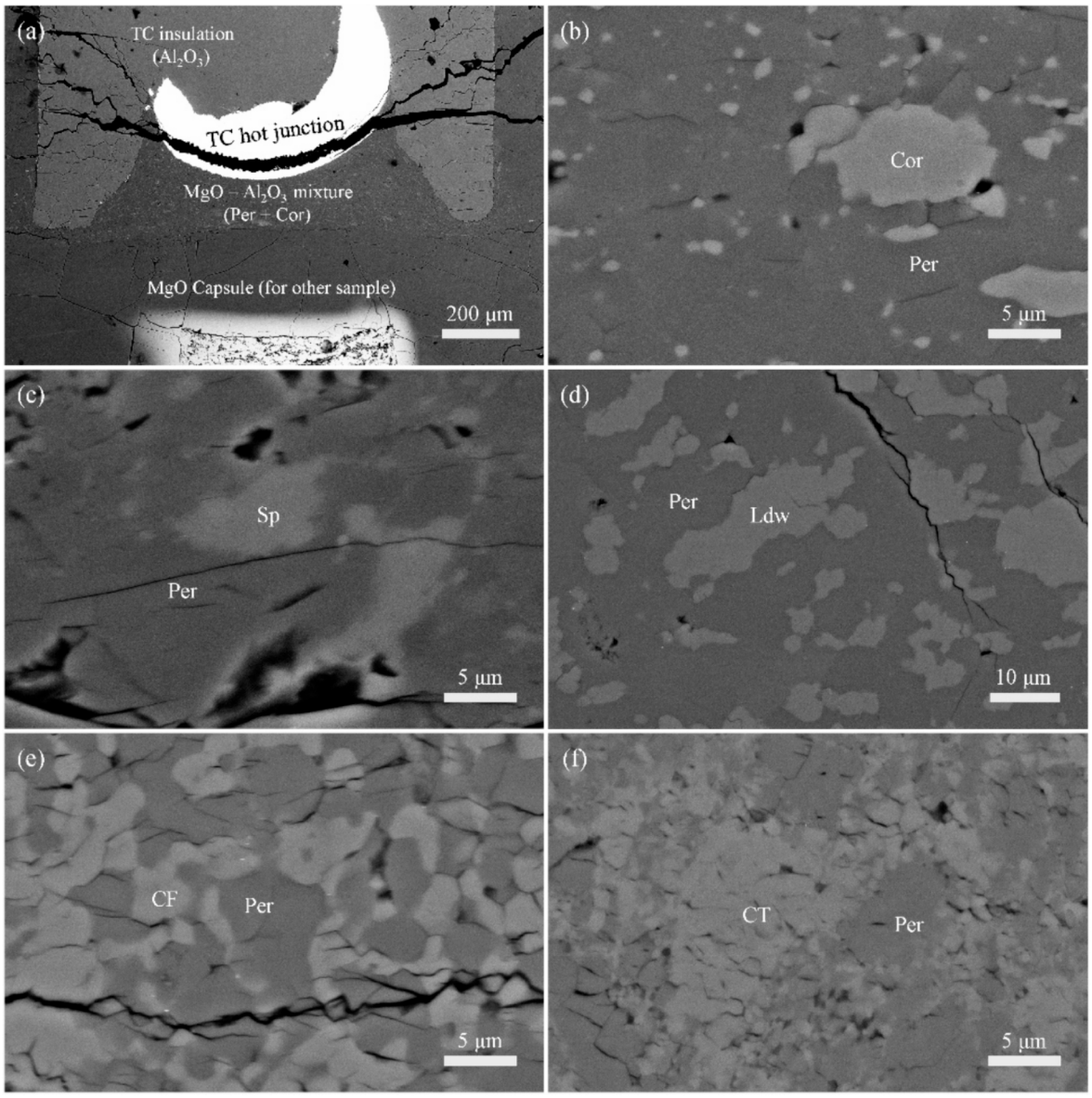


**Fig. 1.** Backscattered electron images of recovered samples. (a) An example where a MgO-$Al_2O_3$ mixture was placed around the thermocouple (TC) junction of a high-pressure assembly. The assembly was recovered from 23 GPa and 1923 K (H5310b). (b) An enlarged portion of the MgO-$Al_2O_3$ mixture located directly under the TC hot junction shown in (a) containing the assemblage periclase (Per) and corundum (Cor). (c) Coexisting periclase (Per) and spinel (Sp) recovered from 15 GPa and 1773 K (H5431b). (d) Coexisting periclase and $Mg_2Al_2O_5$ phase with a modified ludwigite structure (Ldw) recovered from 23 GPa and 2623 K (H5359b). (e) Coexisting periclase and calcium ferrite phase (CF) of $MgAl_2O_4$ recovered from 27 GPa and 2200 K (I1255). (f) Coexisting periclase and calcium titanate (CT) phase of $MgAl_2O_4$ recovered from 50 GPa and 2000 K (I1420).

within 100 μm of the TC junction is reported. For experiments in the FeO-MgO-$Al_2O_3$ system, the capsules were made of four-hole dense polycrystalline $Al_2O_3$ tubes, with 0.2 mm diameter holes. MgO-$Al_2O_3$, Fp90-$Al_2O_3$, Fp80-$Al_2O_3$, and Fp60-$Al_2O_3$ starting materials were placed in each of the holes. Thermocouples were not used in the experiments in the FeO-MgO-$Al_2O_3$ system as a comparison is made with the solubility in the MgO-$Al_2O_3$ sample.

After compression to the target load, a $LaCrO_3$ or rhenium furnace was used to heat the sample to the desired temperatures (1773–2623 K). Samples were heated for between 1 and 1200 min, depending on the P-T conditions, before quenching to room temperature by switching off the heating power and decompressing. After recovery, the assemblies were embedded in epoxy resin and then ground and polished with sandpaper and polishing cloths, utilizing increasingly finer diamond sprays (1 μm, 0.5 μm, and 0.25 μm). The experimental phase assemblages were characterized using a scanning electron microscope (SEM, LEO1530) and a micro-focused powder X-ray diffractometer (Brucker AXS D8 Discover) equipped with a two-dimensional solid-state detector, using a Co-Kα radiation source operated at 40 kV and 500 μA. The chemical compositions of the run products were then quantified using a JEOL JXA-8200 electron probe microanalyzer (EPMA) operating at 15 kV and 15nA. Periclase, corundum, and iron metal were used as standards. Analyses were performed with a focused beam of approximately 1 μm diameter. Simulations on the influence of secondary fluorescence from the adjacent $Al_2O_3$-rich phase on the Al concentration in periclase were performed using the PENEPMA computer program (Llovet and Francesc, 2017). The effect is found to be negligible, as it contributes <0.016 wt% to the periclase analysis when the probe beam is 2 μm away from the grain boundary of an $Al_2O_3$-rich phase, see Supplementary Fig. S1.

## 3. Results

### 3.1. Phase assemblages identified in the MgO-$Al_2O_3$ system experiments

The experimental conditions and run products are listed in Table 1 and images of typical experimental samples are shown in Fig. 1. Diffusion and reaction of MgO or $Al_2O_3$ from the surrounding assembly into the samples was found to be minimal and all runs contained periclase coexisting with an $Al_2O_3$-rich phase, which therefore fixed the $Al_2O_3$ activity. As stated, in most of the experiments the MgO-$Al_2O_3$ sample was placed around the TC junction and a secondary sample was often placed below this, which was used for another purpose. This secondary sample was in some instances FeO-bearing and diffusion of FeO resulted in minor amounts of FeO in the MgO-$Al_2O_3$ samples, which reached values in the range 0.1–0.5 wt% in four samples and 0.9 wt% in one sample (Table 1). As explained later, FeO appears to have very little effect on the $Al_2O_3$ solubility in periclase, especially at these very low concentrations.

The average grain size of periclase in different runs ranged from approximately 5 μm to a little larger than 10 μm, depending on the temperature and heating duration. The chemical composition of periclase is homogenous within single periclase grains and does not show significant chemical zoning. The diffusion coefficients of Al in periclase are expected to be larger than $10^{-13}$ $m^2/s$ under the pressure and temperature conditions in the present experiments (Van Orman et al., 2009). The diffusion length scale of Al in periclase should, therefore, be larger than the typical grain size of 5 μm within 1 min, implying that chemical equilibrium should be rapidly achieved. As the grain size of the starting materials is ~1 μm, the rapid grain growth, even in experiments run for only 10 min at 1773 K, also indicates rapid diffusion of Mg and Al in periclase, therefore, also supporting the attainment of chemical equilibrium in the run products.

The experimental phase relations are plotted in Fig. 2 and compared with the previous estimates of these boundaries. The breakdown of $MgAl_2O_4$ spinel to MgO and $Al_2O_3$ was found to occur between 15 GPa and 19 GPa at temperatures between 1773 K and 2273 K, which agrees well with the phase boundaries established in the experiments of Akaogi et al. (1999) and Kojitani et al. (2010). At temperatures higher than 2273 K at 23 GPa, corundum and periclase recombined to form a $Mg_2Al_2O_5$ modified ludwigite (Ldw) structured phase, which is also consistent with previous studies (Enomoto et al., 2009; Kojitani et al., 2010). The $MgAl_2O_4$ calcium ferrite (CF) structured phase was found at

**Table 1**
Experimental Conditions and Results.

| Run No. | Pressure (GPa) | Temperature (K) | Duration (min) | Coexisting phases[a] | EPMA Measurements on Periclase (wt.%)[b] | | | | | Normalized compositions (mol.%) | | |
|---|---|---|---|---|---|---|---|---|---|---|---|---|
| | | | | | MgO | FeO | $Al_2O_3$ | Total | N | MgO | FeO | $Al_2O_3$ |
| H5431b | 15 | 1773 (50) | 760 | Per, Sp | 99.8 (5) | n. d. | 0.9 (2) | 100.8 (3) | 11 | 99.63 (10) | 0.00 (0) | 0.37 (10) |
| H5424b | 15 | 2073 (50) | 30 | Per, Sp | 96.1 (3) | 0.5 (1) | 3.4 (2) | 100.0 (2) | 5 | 98.33 (14) | 0.30 (8) | 1.37 (8) |
| H5482b | 19 | 1773 (50) | 20 | Per, Cor | 99.1 (3) | 0.0 (0) | 0.5 (1) | 99.6 (3) | 6 | 99.79 (4) | 0.01 (1) | 0.21 (4) |
| H5490b | 19 | 1773 (50) | 10 | Per, Cor | 99.7 (8) | 0.0 (0) | 0.6 (1) | 100.3 (8) | 6 | 99.78 (3) | 0.01 (0) | 0.22 (3) |
| H5492b | 19 | 2073 (50) | 20 | Per, Cor | 97.5 (5) | 0.0 (0) | 2.5 (2) | 100.0 (3) | 7 | 98.98 (2) | 0.02 (2) | 1.00 (8) |
| H5495 | 19 | 2273 (50) | 5 | Per, Cor | 93.4 (8) | 0.0 (0) | 7.1 (7) | 100.6 (5) | 11 | 97.06 (29) | 0.01 (1) | 2.93 (29) |
| H5310b | 23 | 1923 (50) | 360 | Per, Cor | 99.9 (5) | 0.0 (0) | 1.1 (1) | 101.0 (5) | 14 | 99.55 (4) | 0.01 (1) | 0.45 (4) |
| H5306 | 23 | 2073 (50) | 180 | Per, Cor | 98.2 (7) | 0.0 (0) | 2.5 (1) | 100.7 (6) | 5 | 99.01 (3) | 0.01 (0) | 0.98 (4) |
| H5299[c] | 23 | 2273 (50) | 120 | Per, Cor, (Ldw) | 94.7 (5) | 0.0 (0) | 5.4 (2) | 100.1 (5) | 3 | 97.79 (9) | 0.02 (1) | 2.19 (9) |
| I1421c | 27 | 1973 (50) | 10 | Per, Cor | 99.2 (3) | 0.0 (0) | 0.9 (1) | 100.1 (3) | 12 | 99.64 (4) | 0.01 (1) | 0.34 (4) |
| H5420b | 23 | 2373 (50) | 15 | Per, Ldw | 93.0 (7) | 0.9 (7) | 6.6 (4) | 100.6 (4) | 9 | 96.72 (53) | 0.55 (39) | 2.73 (15) |
| H5435b | 23 | 2400 (50) | 5 | Per, Ldw | 90.1 (6) | 0.1 (0) | 8.3 (3) | 98.5 (7) | 15 | 96.42 (13) | 0.06 (2) | 3.52 (12) |
| H5317b | 23 | 2623 (50) | 3 | Per, Ldw | 84.7 (6) | 0.4 (1) | 15.6 (7) | 100.7 (6) | 9 | 92.97 (31) | 0.27 (6) | 6.76 (32) |
| H5359b | 23 | 2623 (50) | 1 | Per, Ldw | 85.4 (6) | 0.0 (0) | 15.0 (7) | 100.4 (4) | 9 | 93.48 (31) | 0.01 (1) | 6.51 (31) |
| H5345b | 23 | 2623 (50) | 1 | Per, Ldw | 86.9 (6) | 0.0 (0) | 14.1 (6) | 101.0 (6) | 13 | 93.97 (25) | 0.01 (1) | 6.02 (25) |
| I1401b | 27 | 1973 (50) | 10 | Per, CF | 100.5 (3) | 0.0 (0) | 0.8 (1) | 101.2 (2) | 11 | 99.70 (4) | 0.01 (1) | 0.29 (4) |
| I1412c | 27 | 2123 (50) | 5 | Per, CF | 99.6 (4) | 0.0 (0) | 1.1 (1) | 100.7 (3) | 16 | 99.54 (5) | 0.01 (1) | 0.45 (4) |
| I1255 | 27 | 2200 (50) | 120 | Per, CF | 97.9 (7) | n. d. | 2.6 (1) | 100.5 (6) | 16 | 98.96 (6) | 0.00 (0) | 1.04 (6) |
| I1193 | 33 | 2000 (50) | 1200 | Per, CF | 96.6 (4) | 0.0 (0) | 0.4 (1) | 97.0 (13) | 9 | 99.81 (6) | 0.02 (3) | 0.17 (4) |
| I1415 | 33 | 2300 (50) | 10 | Per, CF | 98.1 (5) | 0.1 (2) | 1.8 (1) | 100.0 (5) | 11 | 99.23 (13) | 0.06 (2) | 0.71 (4) |
| I1420 | 50 | 2000 (50) | 20 | Per, CT | 100.4 (4) | 0.0 (0) | 0.4 (0) | 100.8 (3) | 13 | 99.85 (2) | 0.01 (0) | 0.15 (4) |

Notes. [a]Abbreviations: Per, periclase; Sp, spinel; Cor, corundum; Ldw, $Mg_2Al_2O_5$ phase with a modified ludwigite structure; CF, calcium ferrite phase of $MgAl_2O_4$; CT, calcium titanate phase of $MgAl_2O_4$. [b]The numbers in parentheses are one standard deviation in terms of least units cited and n. d. is not detectable. N is the number of EPMA-analyses. [c]In run H5299, the TC broke at 2223 K, and the final temperature (2273 K) is extrapolated from the power-temperature relation of the same run. The coexisting phases are Per and Sp near the TC, but the Ldw phase, indicated in the brackets, appears in the hotter region of the assembly.

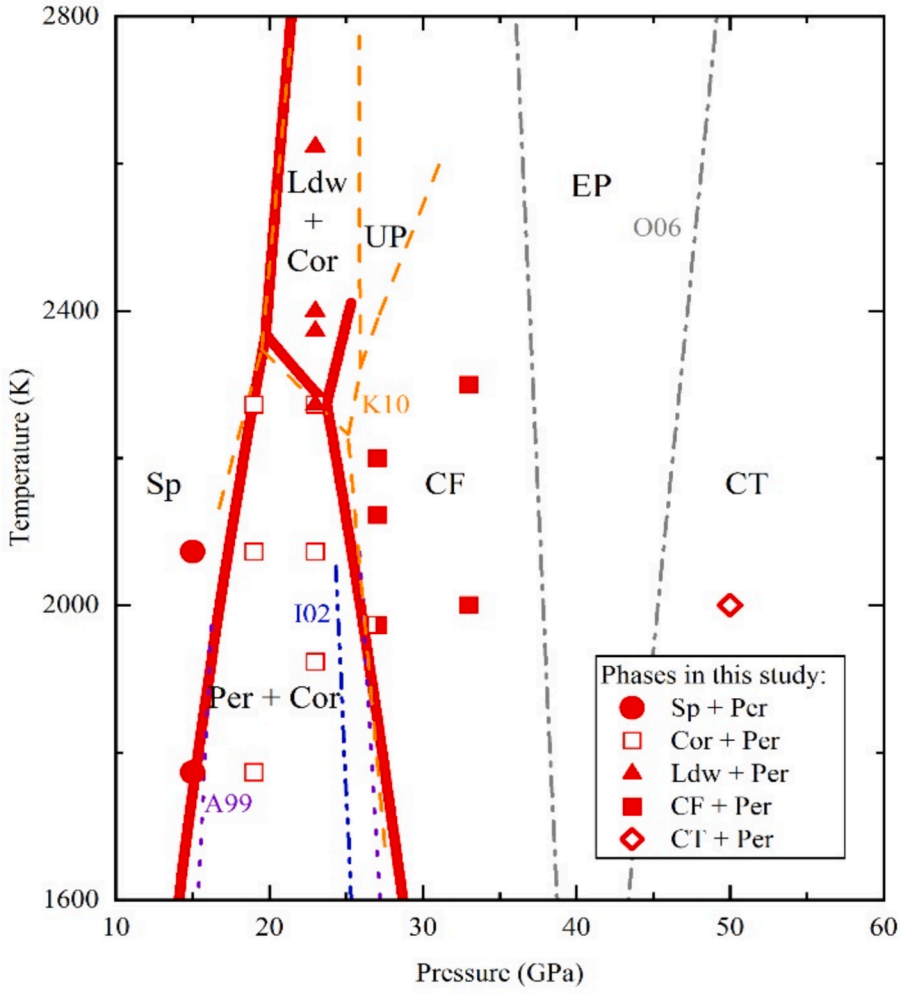


**Fig. 2.** Phase relations in the MgO-$Al_2O_3$ system and the phase assemblages observed at different P-T conditions in this study. Abbreviations are Per, periclase; Sp, spinel; Cor, corundum; Ldw, $Mg_2Al_2O_5$ phase with a modified ludwigite structure; CF, calcium ferrite phase of $MgAl_2O_4$; CT, calcium titanate phase of $MgAl_2O_4$. UP is the $MgAl_2O_4$ phase with an unknown structure discovered by Kojitani et al. (2010) and EP is the ε-type $MgAl_2O_4$ phase found by Liu (1978) and confirmed by Ono et al. (2006). Thick red lines show the phase boundaries calculated from the thermodynamic model described in Section 3.3, where the UP, EP, and CT phases were not considered. The violet dotted lines (A99) indicate the Sp = Per + Cor and Per + Cor = CF phase from Akaogi et al. (1999). The blue dash dotted line (I02) is the phase boundary Per + Cor = CF phase from Irifune et al. (2002). The orange dashed lines (*K*10) are phase boundaries between Sp, Per + Cor, CF, Ldw + Cor, and UP from Kojitani et al. (2010). The grey dash lines (O06) are the phase boundaries between CF/EP and EP/CT determined by Ono et al. (2006). (For interpretation of the references to colour in this figure legend, the reader is referred to the web version of this article.)

pressures of 27 GPa and 33 GPa, consistent with the transition boundary determined by Kojitani et al. (2010). A low-density calcium ferrite phase (LD-CF) identified by Ishii et al. (2021) at 27 GPa and 2773 K and a $MgAl_2O_4$ phase of unknown structure (unknown phase, UP) stable above 26 GPa and 2473 K found by Kojitani et al (2010) were out of the investigated pressure and temperature range of this study. At 50 GPa and 2000 K (I1420), a $MgAl_2O_4$ calcium titanate (CT) phase was identified by powder XRD (Supplementary Fig. S2).

The chemical compositions of the coexisting phases can be found in Table S1. The spinel and CF phase are slightly enriched in MgO, exhibiting an Al/Mg ratio ranging between 1.92 and 1.98. Coexisting corundum contains up to 2.5 mol.% MgO. The composition of the modified ludwigite phase closely aligns with $Mg_2Al_2O_5$ stoichiometry, within the margins of analytical uncertainty. In contrast, the $MgAl_2O_4$ CT phase synthesized at 50 GPa and 2000 K is markedly non-stoichiometric, with an Al/Mg ratio of 1.85.

### 3.2. Solubility of $Al_2O_3$ in periclase

Table 1 and Fig. 3 show the $Al_2O_3$ concentration in periclase coexisting with different Al-rich phases at various P-T conditions. Following the same non-linear trend as the ambient pressure data (e.g., Alper et al., 1962; Stubican and Roy, 1965; Mori, 1982; Zienert and Fabrichnaya, 2013), the solubility of $Al_2O_3$ in periclase increases strongly with temperature. For example, at 23 GPa it increases from 0.45 mol.% at 1923 K to higher than 6.8 mol % at 2623 K. The transition of the coexisting $Al_2O_3$-rich phase from corundum to the $Mg_2Al_2O_5$ ludwigite phase has a near negligible influence on the $Al_2O_3$ solubility in periclase, as the temperature dependence follows an almost identical trend before and after the phase transition at 23 GPa. Overall, pressure suppresses the solubility of $Al_2O_3$ in periclase and decreases its rate of change, i.e., sensitivity, with temperature. For example, an increase in temperature of 100 K at 1 bar and 2000 K raises the solubility by approximately 1.1 mol %, whereas the solubility drops by approximately the same amount if the pressure is increased to 15 GPa, where the temperature sensitivity, i.e., the increase in the periclase $Al_2O_3$ solubility for the same temperature increase, is approximately halved. By 33 GPa the experimentally determined solubilities are < 1 mol % even at the highest temperature investigated, and by 50 GPa the solubility is approximately one order of magnitude lower (0.15 mol.%) than the

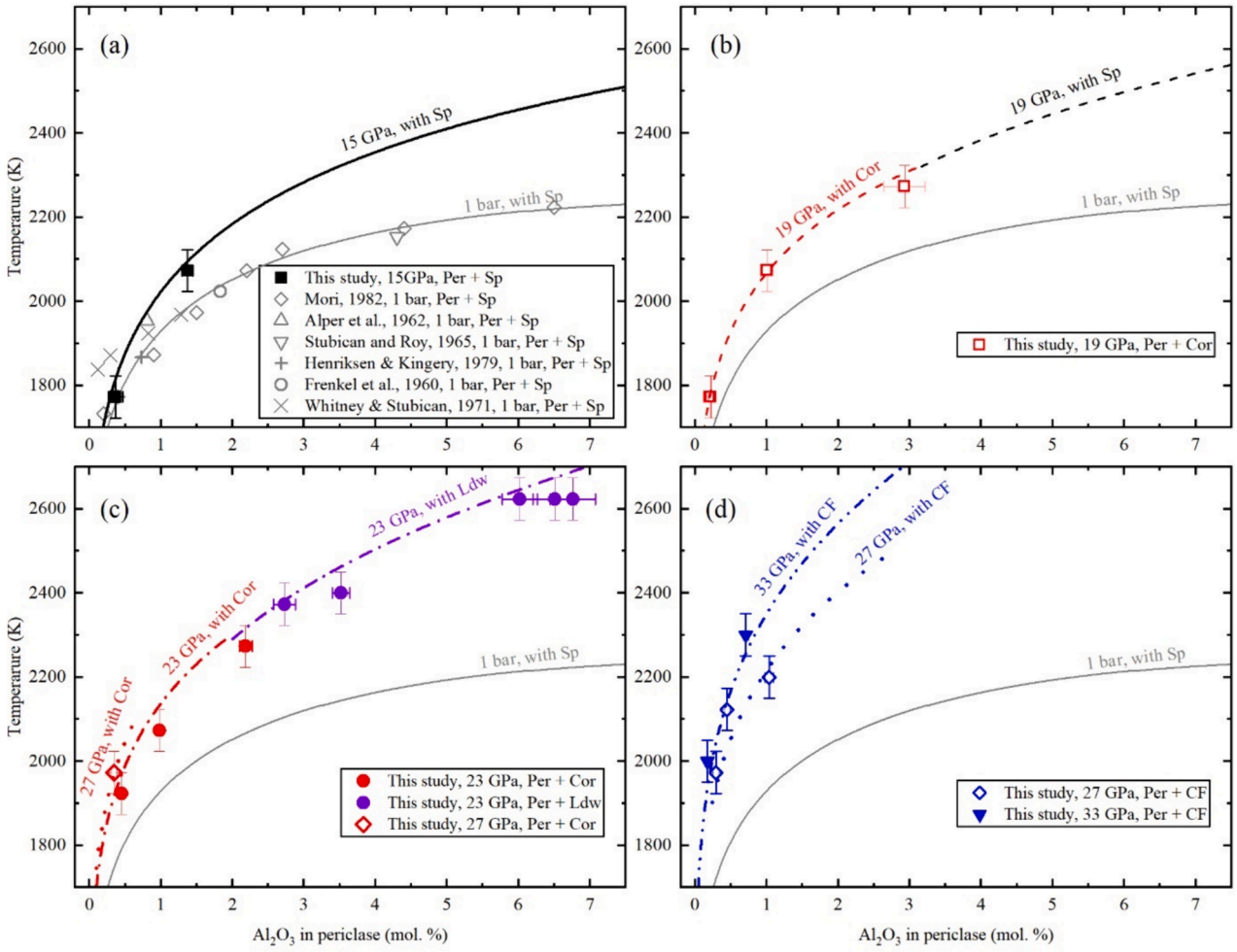


**Fig. 3.** The solubility of $Al_2O_3$ in periclase as a function of pressure and temperature. Experimental results at 15 GPa (a), 19 GPa (b), 23–27 GPa (c), and 27–33 GPa are compared with a thermodynamic model that is fit to the entire dataset, as described in Section 3.3. Results at ambient pressure from the literature (Frenkel et al., 1960; Alper et al., 1962; Stubican and Roy, 1965; Whitney and Stubican, 1971; Henriksen and Kingery, 1979; Mori, 1982) are also plotted for comparison. All curves are calculated considering the indicated coexisting phases at the denoted pressures using the thermodynamic model. The abbreviations are as described for Fig. 2.

ambient pressure value at 2000 K. This pressure dependency is due to the positive volume change that occurs as Al enters periclase from a coexisting phase, which is compounded by the high-pressure phase transitions to increasingly denser phases. As periclase goes through no phase transition at mantle conditions, its $Al_2O_3$ solubility will likely decrease throughout the entire mantle, i.e. up to 135 GPa.

### 3.3. *Thermodynamic modeling of the MgO-$Al_2O_3$ System*

A series of equilibria involving a periclase $AlO_{1.5}$ component are used to fit the experimental data in the MgO-$Al_2O_3$ system over different pressure ranges, depending on the stability of the coexisting $Al_2O_3$-rich phase. In this fitting process thermodynamic terms for the standard state of the $AlO_{1.5}$ component and periclase non-ideal mixing terms are refined. The use of an $AlO_{1.5}$ component is consistent with previous 1 bar treatments (Hallstedt, 1992; Zienert and Fabrichnaya, 2013) and with the models that use an $FeO_{1.5}$ component in wüstite and ferropericlase (Jung et al., 2004; Hidayat et al., 2017). For the thermodynamic properties of coexisting corundum and spinel, which are all treated as single component phases, the database of Holland and Powell (2011) is used. For the $Mg_2Al_2O_5$ modified ludwigite phase, the standard state properties were fitted using the phase relations (Kojitani et al., 2010), employing properties from the Holland and Powell (2011) database for all other phases, with the heat capacity estimated from a summation of values for periclase and corundum. For the CF phase an existing thermodynamic treatment was used (Kojitani et al., 2012). The phase boundaries calculated using these data are shown as the solid curves in Fig. 2 and are in good agreement with phase boundaries bracketed by Kojitani et al. (2010). As the phase boundaries with the CT phase are poorly known, the data point obtained at 50 GPa was not used in the model. To fit the phase equilibria data of Akaogi et al. (1999) and Kojitani et al. (2010) for the breakdown of spinel to periclase and corundum it was necessary to add a $\Delta V$ of disordering to the spinel Bragg-Williams treatment in the Holland and Powell (2011) database. These two previous studies on the phase relations are inconsistent with each other, which is assumed to be caused by metastable persistence of spinel at temperatures <1500 °C in the experiments of Akaogi et al. (1999).

Several studies have examined the Al-content of periclase in equilibrium with spinel at 1 bar (Alper et al., 1962; Stubican and Roy, 1965;

Mori, 1982). From the equilibrium

$$\underset{\text{spinel}}{MgAl_2O_4} \Leftrightarrow \underset{\text{periclase}}{2AlO_{1.5}} + MgO \quad (1)$$

the condition for equilibrium can be rearranged to give

$$-\Delta G^{o}_{(1)} = RTln\left(X^{Per}_{MgO}\right) + 2RTln\left(X^{Per}_{AlO_{1.5}}\right) + W^{Per}_{MgO-AlO_{1.5}}\left[1 - 2X^{Per}_{MgO} + 3\left(X^{Per}_{MgO}\right)^2\right] \quad (2)$$

where $\Delta G^{o}_{(1)}$ is the standard state Gibbs free energy of equilibrium (1), $R$ is the gas constant, $X^{Per}_{AlO_{1.5}}$ is the mole fraction of $AlO_{1.5}$ in periclase, and $W^{Per}_{MgO-AlO_{1.5}}$ is a symmetric Margules interaction parameter that describes the non-ideality of mixing between MgO and $AlO_{1.5}$ in periclase. $W^{Per}_{MgO-AlO_{1.5}}$ is a function of temperature and pressure i.e.,

$$W^{Per}_{MgO-AlO_{1.5}} = W_H - TW_S + PW_V \quad (3)$$

$\Delta G^{o}_{(1)}$ is determined using the Holland and Powell (2011) database except for the $AlO_{1.5}$ component of periclase which is calculated at 1 bar and the temperature of interest from,

$$\Delta_f G^{oPer}_{AlO_{1.5}(1bar,T)} = 0.5\left[\Delta_f G^{oCor}_{Al_2O_3(1bar,T)} + A + BT\right] \quad (4)$$

where $\Delta_f G^{oCor}_{Al_2O_3(1bar,T)}$ is the Gibbs free energy of formation of corundum, calculated from the Holland and Powell (2011) database, and A and B are constants. The terms A, B, $W_H$, and $W_S$ were refined by fitting 1 bar measurements of the Al-content of periclase in equilibrium with spinel (Frenkel et al., 1960; Alper et al., 1962; Stubican and Roy, 1965; Whitney and Stubican, 1971; Henriksen and Kingery, 1979; Mori, 1982) to equation (2). The non-stoichiometric higher MgO content of spinel observed at 1 bar with increasing temperature was ignored as it is relatively small (~5 mol %) and is not observed in the high-pressure data (see Supplementary Table S1). Using a series of equilibria similar to [1], data from experiments where periclase coexists with spinel, corundum, the $Mg_2Al_2O_5$ ludwigite phase and the $MgAl_2O_4$ CF phase, were fitted simultaneously in a weighted least squares procedure by refining the $W_V$ term of the periclase interaction parameter and the volume and bulk modulus of the periclase $AlO_{1.5}$ component. Refinement of the thermal expansion term resulted in unfeasibly high values and it was, therefore, fixed at the value for periclase. The resulting terms are reported in Supplementary Tables S2–S4 and a comparison between the model and the experimental data is shown in Fig. 3. The model well describes both the ambient pressure data from the literature (Frenkel et al., 1960; Alper et al., 1962; Stubican and Roy, 1965; Whitney and Stubican, 1971; Henriksen and Kingery, 1979; Mori, 1982) and the high-pressure data from this study. The discrepancy in temperature between data points and the model are generally within 2 %. The major uncertainty in the experimental data is caused by the temperature gradient in the sample region, even though we chose grains for microprobe analysis that were as close to the thermocouple hot junction as possible. As the hot junction generally extends over at least 0.5 mm in the radial direction and 0.2 mm axially (Fig. 1a), thermocouple readings are likely to be still averages over these regions, even though the high thermal conductivity of the thermocouple wires should alleviate this to some extent. Nevertheless, the difference in temperature between thermocouple readings and actual temperatures of the EPMA analysed region may be up to 50 K. Furthermore, no correction was applied to the thermocouple emf to take account of a potential pressure effect. Although such an effect has been measured for type-D thermocouple (Nishihara et al., 2020), the conditions at which it has been determined are at lower pressures and temperatures than examined here and cannot be safely extrapolated. Any pressure corrections on temperature measurements using type-D thermocouples determined in the future at conditions closer to the experiments performed here, would, therefore, have to be added on to the temperatures determined using $Al_2O_3$ solubility analyses.

The experiment at 50 GPa, where the $MgAl_2O_4$ structured CT phase coexisted with periclase, was not included in the modelling as there are insufficient observations to obtain thermodynamic properties for the CT phase. As shown in Fig. S3, an extrapolation of the model assuming equilibrium with the lower pressure CF phase underestimates the periclase $Al_2O_3$ content at 2000 °C by approximately 0.07 mol %, which is outside of the analytical uncertainty of 0.04 mol %. Although the model is probably consistent once temperature uncertainties are also considered, it is unexpected that fixing the $Al_2O_3$ activity with the CF phase underestimates values in the CT phase stability field, as the latter has a smaller volume and we would, therefore, expect the model to overestimate it (Ono et al., 2006). It is possible that this discrepancy may be explained once reliable data to determine the thermodynamic properties from the phase boundaries becomes available.

Fig. 4 shows the results of the thermodynamic model with the $Al_2O_3$ content of periclase calculated at four different temperatures between ambient pressure and 40 GPa. The sensitivity of the $Al_2O_3$ solubility to temperature is high above 1800 K and increases with temperature, which can be attributed to the effect of the configurational entropy on the $Al_2O_3$ solubility and also due to a decrease in the Margules interaction term. However, the solubility also decreases with pressure, with a steepening in slope occurring upon the phase transformation of spinel to higher-pressure phases. This is an effect of the volume change of the governing equilibrium and is most likely caused by a change in site occupancy of Al, from partial tetrahedral occupancy in spinel to complete octahedral occupancy in corundum and the ludwigite structure. Periclase $Al_2O_3$ solubility could be applied as a thermometer and/or barometer in high pressure multi-anvil experiments, or in other high-pressure equipment. This might be useful, for example, in experiments where the thermocouple has broken, perhaps during studies of high-pressure melting phase relations. Very small amounts of MgO-$Al_2O_3$ mixtures could be added to the high-pressure assembly and then analysed afterwards to extract the temperature. At 2100 K and 15 GPa, for example, a 0.1 mol % difference in $Al_2O_3$ content, which is easily measurable, equates to a temperature difference of only 20 K. Whereas if the pressure at these conditions was uncertain by 2 GPa, this equates to a change in solubility of only 0.05 mol %, i.e., a 10 K uncertainty on the absolute temperature determination. The accuracy of such absolute temperature determinations increases with temperature but decreases with pressure and would become inaccurate above 27 GPa, where the solubility becomes low and small changes equate to large temperature changes. On the other hand, if the temperature were to be measured using a thermocouple, then at temperatures above 2200 K the solubility could be used to provide a quite accurate pressure determination, also with a practical limit of approximately 27 GPa, although potentially higher for experiments performed at the volatile-free silicate solidus.

### 3.4. Further experiments on the effect of FeO on ferropericlase $Al_2O_3$ solubility

Two experiments (H5874, H5875) were conducted in the FeO-MgO-$Al_2O_3$ system at 21 GPa and temperatures of approximately 2000 and

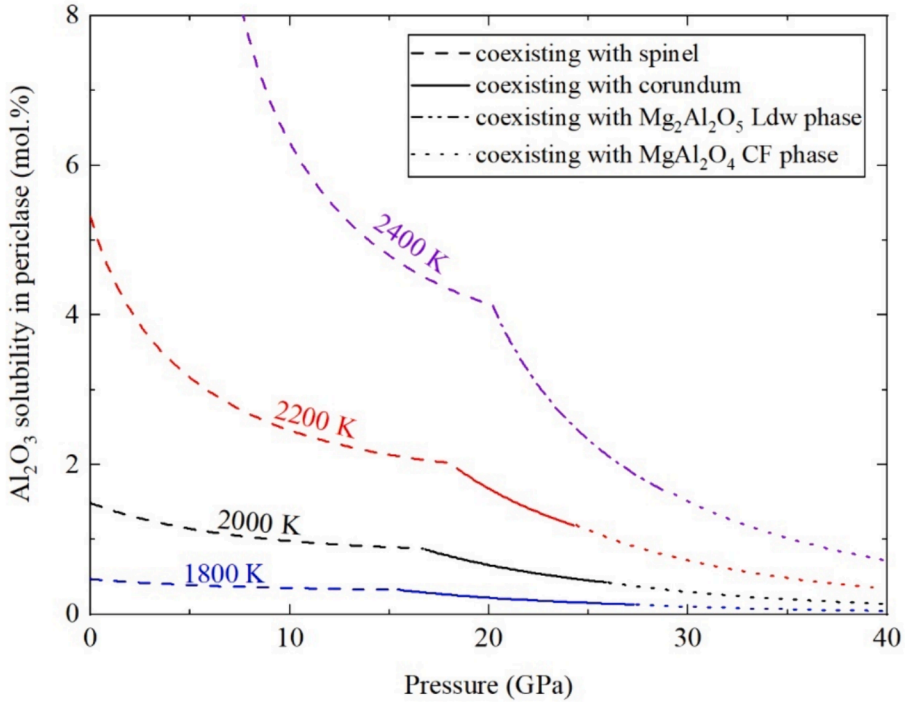


**Fig. 4.** $Al_2O_3$ solubility in periclase as a function of pressure in the MgO-$Al_2O_3$ system calculated using the derived thermodynamic model. The coexisting phases are indicated by the type of dashed and solid lines. The abbreviations are as described for Fig. 2.

2200 K respectively. As these experiments were performed to examine the effect of FeO on ferropericlase $Al_2O_3$ solubility at the same temperatures, no thermocouple was employed and temperatures are simply compared to those obtained from the MgO-$Al_2O_3$ sample in the same experiment. The run products of the four compositions in both experiments are periclase or ferropericlase coexisting with corundum (see Fig. 5 and Fig. S4). Grains of metallic iron remained in all recovered samples from the FeO-bearing starting compositions, ensuring minimal ferric iron. The FeO concentrations in the ferropericlase samples are a few mole percent higher than in the starting materials (see Fig. 5 and Table 2), due to oxidation of metallic iron, most likely, by absorbed water in the starting materials and ceramic assembly components. The capsule containing the four samples was ground and exposed perpendicular to the axial direction of the furnace, close to the upper surface (end). As each sample is located at an approximately symmetric position, they should each have experienced the same temperature. Run H5875 was then ground down a second time by a further 0.3 mm to expose the four samples closer to the center of the capsule in the axial direction, which experienced a higher temperature (center) than at the end of the capsule. As shown in Fig. 5a, compared to the FeO-free end-member, the presence of up to 44 mol.% FeO in ferropericlase results in only a minor variation in ferropericlase $Al_2O_3$ solubility. In run H5874, for which the end-member periclase $Al_2O_3$ solubility gives a T of 2124 ± 20 K, with the uncertainty propagated only from the compositional variation, the ferropericlase samples have identical $Al_2O_3$ solubilities within the analytical uncertainty (~0.1 mol.%). For the end of the sample in run H5875, the periclase solubility gives a T of 2235 ± 13 K, whereas the more FeO-rich samples have slightly lower solubilites. Nevertheless, the T calculated for the ferropericlase samples are still at most only 42 K lower. At the center of the same sample the T is 2299 ± 11 K, and the FeO-samples again record temperatures that are only 45 K lower. Given that the apparent effect of FeO on the ferropericlase $Al_2O_3$ solubility only seems to appear once the temperature is raised above approximately 2100 K, is seems more plausible that the FeO-samples at these higher temperatures are indeed recoding small radial temperature variations in the assembly, rather than an effect of FeO on the $Al_2O_3$ solubility. Even if there were an effect of FeO it appears to be insignificant at temperatures below 2100 K and at higher temperatures would cause differences in temperature of < 50 K for FeO contents up to 44 mol.% FeO. We consider, therefore, that for most practical applications the effect of FeO on the $Al_2O_3$ solubility in ferropericlase can be ignored.

## 4. Discussion

### 4.1. Maximum $Al_2O_3$ contents in ferropericlase in the mantle

Before examining ferropericlase $Al_2O_3$ contents in natural systems, it is important to consider whether the presence of other components may influence the $Al_2O_3$ solubilities. The only component present in sufficient proportions to affect $Al_2O_3$ solubility in natural diamond inclusions is FeO, and even this effect appears to be relatively minor, as previously discussed. $Cr_2O_3$ shows the second highest concentrations that can reach values of ~2 wt%, but the $Al_2O_3$-$Cr_2O_3$ interaction parameters would have to be extremely large for such concentrations to influence the $Al_2O_3$ content and this seems not to be the case for other solid solutions such as spinel or garnet (O'Neill and Wall, 1987; Luth et al., 1990). The same argument can be used to discount the effects of other minor components. The $Fe^{3+}/\sum Fe$ ratios in ferropericlase inclusions found in natural diamonds are typically lower than 0.12, and less than 0.05 $Fe^{3+}$ per 1 oxygen formula unit and are therefore unlikely to have any influence (McCammon et al., 1997; McCammon et al., 2004; Kaminsky et al., 2015; Kiseeva et al., 2022). It might be considered that Na could influence the Al content through a charge balanced substitution. However, the Na contents of natural ferropericlase inclusions in diamonds are at most ~1 wt% and as a result the Na-Al interaction parameter would have to be extremely large for an effect on $Al_2O_3$ solubility to be produced. Such a substitution is also clearly not required for large amounts of Al to be accommodated in the periclase and ferropericlase structures.

To determine how periclase $Al_2O_3$ solubility would change within assemblages that might form in the mantle, we have to consider which Al-rich phases will coexist with periclase in the MgO-$Al_2O_3$-$SiO_2$ system,

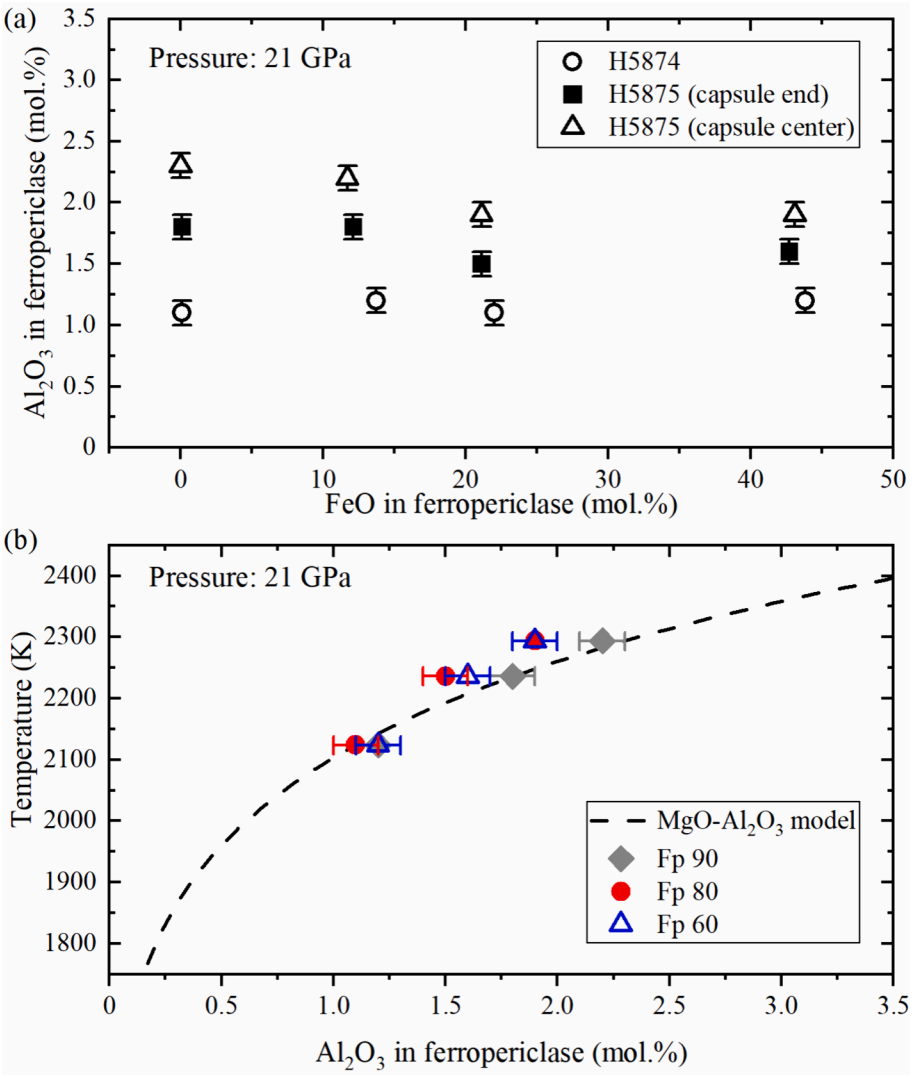


**Fig. 5.** The solubility of $Al_2O_3$ in ferropericlase at 21 GPa. (a) The $Al_2O_3$ solubility is plotted as a function of the FeO content in ferropericlase. (b) The $Al_2O_3$ solubilities are plotted as a function of temperature determined from the periclase sample, assuming that all four samples in each capsule experienced the same temperature.

**Table 2**
Chemical Compositions of Periclase and Ferropericlase in Runs H5874 and H5875.

| Run No.[a] | P (GPa) | Starting materials[b] | EPMA Measurements (wt.%)[c] | | | | | Normalized compositions (mol.%) | | |
|---|---|---|---|---|---|---|---|---|---|---|
| | | | MgO | FeO | $Al_2O_3$ | Total | N | MgO | FeO | $Al_2O_3$ |
| H5874a | 21 | Fp100 + $Al_2O_3$ | 94.9 (3) | 0.2 (0) | 2.7 (1) | 97.8 (2) | 8 | 98.8 (5) | 0.1 (0) | 1.1 (1) |
| H5874b | 21 | Fp90 + $Al_2O_3$ + Fe | 74.9 (3) | 21.5 (2) | 2.6 (1) | 99.0 (2) | 9 | 85.1 (1) | 13.7 (1) | 1.2 (0) |
| H5874c | 21 | Fp80 + $Al_2O_3$ + Fe | 64.5 (3) | 32.9 (3) | 2.4 (1) | 99.8 (3) | 9 | 76.8 (2) | 22.0 (2) | 1.1 (0) |
| H5874d | 21 | Fp60 + $Al_2O_3$ + Fe | 40.8 (3) | 57.8 (4) | 2.2 (1) | 100.8 (4) | 8 | 55.0 (3) | 43.8 (3) | 1.2 (1) |
| H5875a (end) | 21 | Fp100 + $Al_2O_3$ | 93.0 (3) | 0.2 (0) | 4.2 (1) | 97.5 (3) | 8 | 98.1 (1) | 0.1 (0) | 1.8 (1) |
| H5875b (end) | 21 | Fp90 + $Al_2O_3$ + Fe | 76.2 (4) | 19.1 (5) | 3.9 (2) | 99.3 (3) | 9 | 86.2 (3) | 12.1 (3) | 1.8 (1) |
| H5875c (end) | 21 | Fp80 + $Al_2O_3$ + Fe | 65.2 (2) | 31.7 (2) | 3.3 (1) | 100.1 (3) | 11 | 77.4 (1) | 21.1 (1) | 1.5 (1) |
| H5875d (end) | 21 | Fp60 + $Al_2O_3$ + Fe | 41.3 (1) | 56.4 (3) | 3.0 (1) | 100.6 (4) | 9 | 55.7 (1) | 42.7 (1) | 1.6 (1) |
| H5875a (center) | 21 | Fp100 + $Al_2O_3$ | 92.0 (2) | 0.1 (0) | 5.5 (2) | 97.5 (2) | 10 | 97.7 (1) | 0.0(0) | 2.3 (1) |
| H5875b (center) | 21 | Fp90 + $Al_2O_3$ + Fe | 75.8 (3) | 18.3 (3) | 4.8 (2) | 98.9 (3) | 15 | 86.2 (1) | 11.7 (2) | 2.2 (1) |
| H5875c (center) | 21 | Fp80 + $Al_2O_3$ + Fe | 64.4 (3) | 31.4 (3) | 4.0 (2) | 99.8 (4) | 17 | 77.0 (1) | 21.1 (2) | 1.9 (1) |
| H5875d (center) | 21 | Fp60 + $Al_2O_3$ + Fe | 40.5 (2) | 56.4 (4) | 3.5 (1) | 100.4 (3) | 18 | 55.1 (2) | 43.1 (3) | 1.9 (1) |

[a] "end" and "center" indicate the measured surfaces that were close to the end or the center of the capsule perpendicular to the axial direction.
[b] Fp is ferropericlase, with Fp90 indicating, for example, 90 mol % MgO.
[c] The numbers in parentheses are one standard deviation and N is the number of analyses.

as they will fix the $Al_2O_3$ activity. In Fig. 6a, solubilities are calculated for both the MgO-$Al_2O_3$ and MgO-$Al_2O_3$-$SiO_2$ systems at temperatures along a typical mantle adiabat (Katsura, 2022). The latent heat effect of the phase transitions has been smoothed out in this profile (see Supplementary Fig. S5). For the MgO-$Al_2O_3$ system the effects of pressure and temperature result in a maximum $Al_2O_3$ solubility of approximately

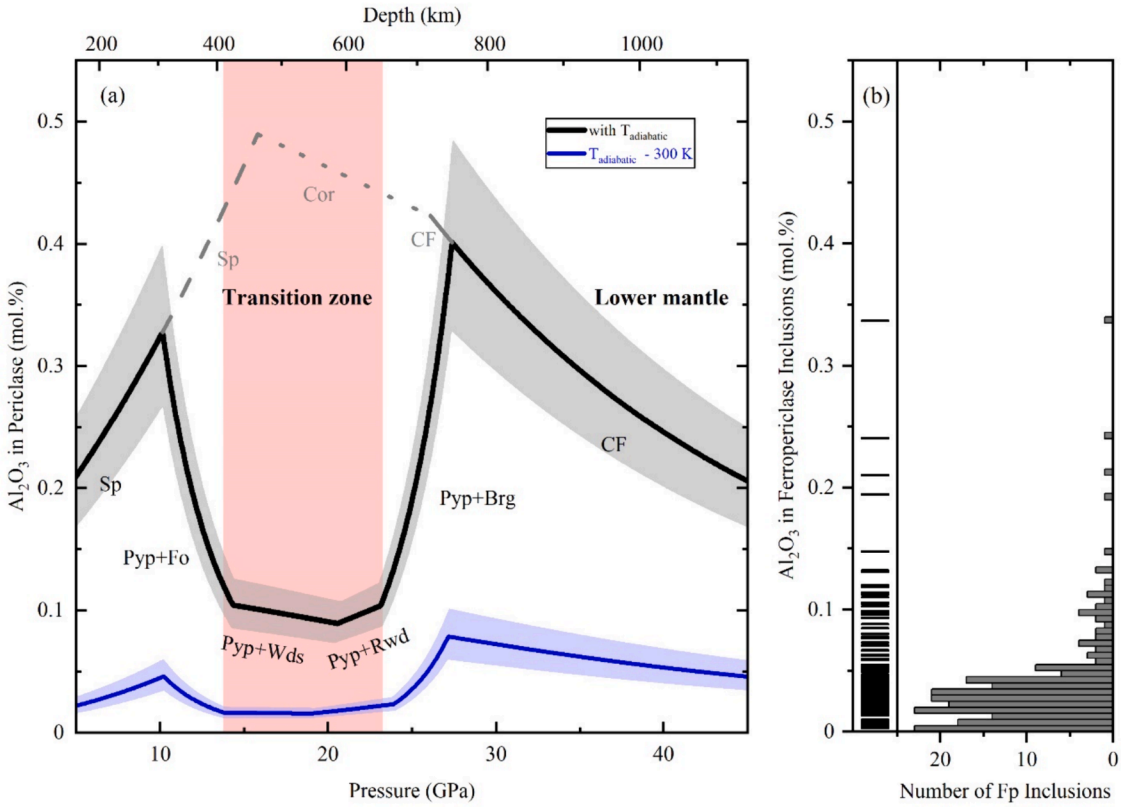


**Fig. 6.** (a) $Al_2O_3$ solubility in periclase in the MgO-$SiO_2$-$Al_2O_3$ and MgO-$Al_2O_3$ systems calculated from the thermodynamic model. The black solid curve shows the calculated periclase $Al_2O_3$ concentration in the MgO-$SiO_2$-$Al_2O_3$ system coexisting with an Al-bearing mineral stable in the mantle at different depths, i.e., spinel (Sp), pyrope (Pyp), or $MgAl_2O_4$ CF phase, along a typical adiabatic mantle temperature (Katsura, 2022). Fo, Wds, and Rwd indicate the polymorphs of $Mg_2SiO_4$, forsterite, wadsleyite, and ringwoodite, respectively. Brg stands for the bridgmanite $MgSiO_3$ endmember. The dashed, dot, and solid grey curves show the maximum $Al_2O_3$ in periclase in the MgO-$Al_2O_3$ system, coexisting with Sp, corundum (Cor), and CF phase, respectively along the same adiabat. The solid blue line shows the periclase $Al_2O_3$ solubility in the MgO-$SiO_2$-$Al_2O_3$ system when the temperatures are 300 K lower than the mantle adiabat. The shaded regions indicate the uncertainties propagated from that of the adiabatic temperature. (b) The compositional distribution of $Al_2O_3$ contents in ferropericlase inclusions in diamonds, from Walter et al. (2022), Seitz et al. (2018), Nimis et al. (2019), Gu et al. (2022), Kiseeva et al. (2022) and Lorenzon et al. (2023). (For interpretation of the references to colour in this figure legend, the reader is referred to the web version of this article.)

0.5 mol % being reached at the spinel to corundum transition near 16 GPa. At this point the strongly temperature dependent solubility in the spinel field gives way to the stronger pressure dependence in the corundum field. If a solubility of this magnitude were found in a ferropericlase inclusion in a diamond, this would imply either adiabatic conditions near the top of the transitions zone, assuming the $Al_2O_3$ activity were set by equilibrium with corundum or pure spinel, or super-adiabatic conditions over a broader depth interval, if we assume that the $Al_2O_3$ activity was actually lower than this. This maximum will only exist in an $SiO_2$-free system however. In the MgO-$Al_2O_3$-$SiO_2$ system, thermodynamic calculation shows that spinel is in equilibrium with periclase only to approximately 10 GPa, where it transforms to pyrope through the reaction:

$$\underset{\text{spinel}}{MgAl_2O_4} + \underset{\text{forsterite}}{3Mg_2SiO_4} = \underset{\text{periclase}}{4MgO} + \underset{\text{pyrope}}{Mg_3Al_2Si_3O_{12}} \quad (5)$$

It is interesting to note that in the presence of periclase, the transformation to produce pyrope is displaced to much higher pressures than in peridotite mantle. In peridotite mantle the pyrope-forming reaction involves enstatite and occurs at approximately 1.5 GPa, but in the presence of excess periclase, enstatite is unstable with respect to forsterite. In the presence of pyrope the $Al_2O_3$ activity drops sharply with pressure, as calculated from the equilibrium,

$$\underset{\text{periclase}}{3MgO} + \underset{\text{pyrope}}{Mg_3Al_2Si_3O_{12}} \Leftrightarrow \underset{\text{forsterite}}{3Mg_2SiO_4} + \underset{\text{periclase}}{Al_2O_3} \quad (6)$$

and at higher pressures from similar equilibria involving wadsleyite and ringwoodite (high pressure polymorphs of forsterite). The presence of periclase means that there is no majoritic component in garnet at transition zone conditions because there is no $MgSiO_3$ component as it reacts with periclase to produce an $Mg_2SiO_4$ polymorph. This is actually consistent with analyses of garnet inclusions in natural diamonds that are considered to be co-occurring with ferropericlase inclusions and which indeed show no majorite component (Walter et al., 2022; Hutchison, 1997).

As ringwoodite breaks down to periclase and bridgmanite at high pressure, the periclase Al-content is calculated to rise very rapidly due to the volume change of the equilibrium. We can again calculate the maximum plausible Al-content in periclase by using the pyrope end-member in the calculations:

$$\underset{\text{pyrope}}{Mg_3Al_2Si_3O_{12}} \Leftrightarrow \underset{\text{bridgmanite}}{3MgSiO_3} + \underset{\text{periclase}}{Al_2O_3} \quad (7)$$

At approximately 26 GPa pyrope will then break down (Ishii et al., 2023) and the CF-$MgAl_2O_4$ phase will become the most $Al_2O_3$-rich phase that can coexist with ferropericlase in the lower mantle. In a peridotite composition the bridgmanite $Al_2O_3$ content would fix the activity of $Al_2O_3$, but this would result in periclase $Al_2O_3$ solubilities lower than those indicated for coexistence with the CF phase. Although higher pressure $MgAl_2O_4$ polymorphs including the CT-phase are not considered in the model, as they are increasingly denser, they should lead to even lower ferropericlase $Al_2O_3$ contents compared to the CF phase

field. The results on the CT phase discussed in Section 3.3 are in general agreement with this, even if they do not agree perfectly with the extrapolation of the CF model. Therefore, the CF curve in Fig. 6a still provides a conservative maximum plausible ferropericlase $Al_2O_3$ content along a mantle adiabat.

The $Al_2O_3$ concentrations in periclase coexisting with bridgmanite in the MgO-$SiO_2$-$Al_2O_3$ system reported by Liu et al. (2019a, 2019b) at 27 GPa are in good agreement with our calculated values. As discussed previously, the effect of FeO and other components should be minimal on the ferropericlase $Al_2O_3$ contents and in fact experimentally determined values reported for ferropericlase coexisting with garnet and bridgmanite are in good agreement with those predicted in Fig. 6a (Frost and Langenhorst, 2002; Huang et al., 2021). Data from Irifune (1994) and Irifune et al. (2010) are also in good agreement with our calculations and document a sharp increase in ferropericalse $Al_2O_3$ concentration at the top of the lower mantle, as calculated in the model. However, some of the reported ferropericlase compositions have $SiO_2$ contents $\geq$1 wt%, which correlate with higher $Al_2O_3$ contents and likely arise from beam overlap with silicate phases.

Our thermodynamic calculations reveal that, under current adiabatic mantle temperatures, the $Al_2O_3$ content in mantle ferropericlase cannot exceed 0.5 mol.%, when uncertainties are considered. While such a minor impurity content will not noticeably affect the thermodynamic or thermoelastic properties of ferropericlase, it could conceivably influence transport properties. As the self-diffusion of Mg in periclase is sensitive to its $Al_2O_3$ content (e.g., Van Orman et al., 2003, 2009; Ammann et al., 2012; Riet et al., 2020), the influence of $Al_2O_3$ on the rate of chemical diffusion in lower mantle ferropericlase may have implications for other transport properties, such as rheology. Furthermore, as the $Al_2O_3$-content in ferropericlase diminishes with increasing depth in the lower mantle, as shown in Fig. 6a, this may, therefore, suppress cation diffusion in periclase in the deep lower mantle. In conjunction with the negative pressure dependence of self-diffusion coefficients in pure periclase (e.g., Ita and Cohen, 1998), bulk chemical transport in the deep lower mantle may be substantially slower compared to the uppermost parts of the lower mantle, with the exception of the core-mantle boundary, where elevated temperatures could accelerate this transport.

### 4.2. *Interpreting the $Al_2O_3$ contents of ferropericlase inclusions in natural diamonds*

Fig. 6b plots the $Al_2O_3$ compositional distribution of natural ferropericlase inclusions in diamonds from the recent review of Walter et al. (2022), and a few other studies (Seitz et al., 2018; Nimis et al., 2019; Gu et al., 2022; Kiseeva et al., 2022; Lorenzon et al., 2023). The $Al_2O_3$ concentration of the inclusions varies between 0 and approximately 0.35 mol.% (0.5 wt%), with an average value close to 0.04 mol.% (0.1 wt%). As discussed previously it is unlikely that the FeO content of ferropericlase has a significant effect on the $Al_2O_3$ solubility so we assume solubilities are the same as for periclase. In this scenario, the concentration of $Al_2O_3$ is a sensor for $Al_2O_3$ activity, temperature, and pressure, with differing sensitivities under different conditions. It can, in principle, be used to constrain any of these three factors if the other two are known, and would, therefore, be more powerful in combination with other methods. If the $Al_2O_3$ activity could be isolated, independently, for example, at a particular pressure and temperature this would provide important information on the chemical environment in which the inclusion formed. Even in the absence of other methods, however, some conclusions can be made on natural samples by making certain reasonable assumptions. Two approaches can be taken, firstly for estimating the conditions of ferropericlase formation and secondly for excluding certain conditions for high-$Al_2O_3$ bearing inclusions. Before employing compositions of natural samples, it should be pointed out that probably none of the available analyses were performed to specifically determine the ferropericlase $Al_2O_3$-content and in some studies, it was not even analysed. Furthermore, in most studies the uncertainties are not reported, and neither can it be clarified that the reported Al-contents originate from ferropericlase and not from other inclusions. In fact, one value reported by Burnham et al (2016) of 8.38 wt% $Al_2O_3$, (with a similar level of $SiO_2$), can most likely be excluded on these grounds. There is also evidence for Al-spinel exsolution from ferropericlase (Wirth et al., 2014), and if such exsolution annealed up after entrapment it might result in misleading or inhomogeneous $Al_2O_3$ contents.

Nonetheless, taking the analyses at face value and employing the first approach, we can examine inclusions that are reported to co-occur with $Al_2O_3$-rich phases and calculate a temperature assuming equilibrium with these phases. Hutchison (1997), for example, reports that ferropericlase inclusion BZ243B co-occurs with pyrope-rich garnet and olivine. Assuming the olivine has not back transformed from a higher-pressure polymorph, then the formation pressure would have been between 10 and 14 GPa. As shown in Fig. 6a, the $Al_2O_3$ solubility changes strongly with pressure under these conditions resulting in formation conditions that vary along a curve extending from 1447 K at 10 GPa to 1680 K at 14 GPa. Hutchison et al. (2004), intriguingly, report a corundum inclusion which is proposed to be associated with ferropericlase (BZ241A). If these phases were indeed in equilibrium then this implies equilibration conditions between 1507 K at 16 GPa and 1597 K at 26 GPa. Harte (1999) on the other hand report that ferropericlase BZ207B co-occurs with proposed bridgmanite, which back-transformed on decompression, and jeffbenite, which may be back-transformed from pyrope (Nestola et al., 2023c). The low Al-content of the proposed bridgmanite limits the pressure to the top of the lower mantle and if we assume pressures of 24–25 GPa, and that jeffbenite was indeed back-transformed from pyrope, we obtain temperatures of between 1800 and 1664 K respectively. As these examples show, to narrow the determined temperatures it would be necessary to obtain an independent measure of the pressure.

Recently, Gu et al. (2022) reported an inclusion assemblage containing touching grains of ringwoodite, ferropericlase, and enstatite, where the enstatite grain was proposed to have been originally trapped as bridgmanite. Based on the Fe-Mg partitioning between ferropericlase and proposed bridgmanite, conditions of ~24 GPa and 1928 $\pm$ 200 K were obtained. Nestola et al. (2023a) investigated a ferropericlase inclusion inside the same diamond using elastic geobarometry and obtained a quite consistent formation pressure of at least 22.1 ($\pm$2.1) GPa. We can make a temperature estimate for the inclusion reported by Gu et al. (2022) using the $Al_2O_3$ contents of the ferropericlase and the coexisting former bridgmanite inclusion, by equating the Gibbs free energies of the $Al_2O_3$ components in the two phases. In the particular inclusion, the bridgmanite FeO and $Al_2O_3$ contents are quite low, approximately 4.5 and 1.2 wt% respectively and a coupled substitution of Al onto the two bridgmanite cation sites is, therefore, plausible (Huang et al., 2021). Using thermodynamic data for the bridgmanite $Al_2O_3$ component and an interaction parameter for bridgmanite $MgSiO_3$-$Al_2O_3$ mixing (reported in Supplementary Tables S2 and S3) derived by fitting coexisting compositions of bridgmanite and corundum determined by Liu et al (2017), we calculate a formation temperature of between 1987 K and 2099 K for pressures of 22.1 and 24 GPa respectively, which is in quite good agreement with the estimates of Gu et al. (2022). To give some idea of the uncertainty, the same calculation using the thermodynamic data of Stixrude and Lithgow-Bertelloni (2022) for the bridgmanite $Al_2O_3$ component gives temperatures that are approximately 150 K lower. If ideal mixing is assumed, all temperature estimates increase by 100 K. This is an interesting result because it not only indicates temperatures which are near or even possibly above a typical mantle adiabat at the top of the lower mantle, but the bridgmanite composition indicates $Al_2O_3$ activities that are relatively low, i.e. lower than those expected for typical mantle peridotite assemblages. As the bulk of ferropericlase inclusions have $Al_2O_3$ contents close to this low level (Fig. 6b) this might imply that they are in general formed at low $Al_2O_3$ activity rather than low temperatures. What is not clear, however,

is why the assemblage reported by Gu et al. (2022) did not chemically reequilibrate during the journey to the lithosphere and then surface.

In the second approach, however, we can exclude conditions of formation of some inclusions where their $Al_2O_3$ contents would be higher than the calculated solubility in the MgO-$SiO_2$-$Al_2O_3$ system at those conditions. This of course works mainly for the highest $Al_2O_3$ bearing samples. The solubility calculated in the MgO-$SiO_2$-$Al_2O_3$ system in Fig. 6a should reflect the highest $Al_2O_3$ activity that can be obtained at any particular pressure and temperature. It is quite plausible that ferropericlase inclusions formed in the mantle under conditions where $Al_2O_3$-activities were lower than those implied by the coexistence of Al-rich phases. In some instances, for example, ferropericlase inclusions appear to co-occur with low-Al bearing chromite spinel (e.g. Kaminsky et al., 2001) that would impose $Al_2O_3$ activities much lower than implied by the curves in Fig. 6a. Similarly, the bridgmanite discussed in the last paragraph had an Al-content much lower than expected for a peridotite bulk composition. Therefore, even low ferropericlase $Al_2O_3$ contents could still equate to high temperatures of formation. However, ferropericlase $Al_2O_3$ contents cannot be higher than the calculated curves in Fig. 6a at any given pressure, unless temperatures were super adiabatic. Furthermore, the addition of FeO to the system has been shown to have an insignificant effect on $Al_2O_3$ solubility and further components such as CaO are hardly soluble in ferropericlase and will only serve to further lower the $Al_2O_3$ activity of the coexisting phase.

As shown in Fig. 6a, periclase $Al_2O_3$ solubility drops significantly in the mantle transition zone. This means that approximately eight of the most Al-rich ferropericlase inclusions can be excluded from forming in the mantle transition zone, unless temperatures were significantly higher than a typical mantle adiabat. These inclusions most likely formed either within a narrow pressure range around 10 GPa or in the top region of the lower mantle. However, these inclusions cannot have formed at temperatures more than 100 K lower than adiabatic temperatures, regardless of where they were produced. This is, therefore, good evidence that at least some diamonds did not form at low temperatures associated with either thick cratonic lithosphere or subduction zones, but at temperatures very close to those of the convecting mantle.

Several studies have proposed that ferropericlase-bearing diamonds may form in the mid-transition zone as carbonate melts released from a subducting slab are reduced on entering the ultramafic mantle (Thomson et al., 2016; Walter et al., 2022). Fig. 6a also shows the same maximum periclase Al-content curves calculated for a temperature profile 300 K below an adiabatic gradient, in order to approximate temperatures close to a subducting slab. The majority of ferropericlase inclusions have $Al_2O_3$-contents that would be quite consistent with such conditions in the transition zone, if they formed in equilibrium with garnet. They could of course, however, have formed at higher temperatures, if $Al_2O_3$ activities were lower.

The $Al_2O_3$ content of ferropericlase inclusions can, therefore, be used to eliminate certain conditions for a subset of higher-Al bearing inclusions but the concentration on its own cannot provide a definitive answer regarding specific formation conditions. A more reliable approach is to use coexisting Al-bearing phases to constrain the $Al_2O_3$ activity and this can then be used to obtain temperatures through the use of an independent method to determine pressure, such as elastic thermobarometry (Anzolini et al., 2019; Kohn et al., 2023). It is also possible that other minor elements in ferropericlase inclusions can yield information on the formation conditions, using a similar type of calibration as performed here. The $SiO_2$ concentration, for example, is generally of a similar magnitude in natural ferropericlase inclusions (Walter et al., 2022) to the $Al_2O_3$ content. Such analyses are important as they provide one of the only mechanisms through which to determine temperatures in the sublithospheric mantle.

## 5. Conclusions

In this study, we have investigated the solubility of $Al_2O_3$ in periclase coexisting with a series of $Al_2O_3$-rich phases formed by high pressure and temperature phase transitions of $MgAl_2O_4$ spinel in the MgO-$Al_2O_3$ system. Experiments were performed at pressures up to 50 GPa and temperatures to 2623 K. The solubility of $Al_2O_3$ in periclase is temperature dependent with the sensitivity to $Al_2O_3$ content increasing with temperature but also decreasing with pressure. A thermodynamic model for periclase $Al_2O_3$ solubility uses the known phase transformation boundaries for $Al_2O_3$-rich phases in the system to determine their thermodynamic properties. This only works to conditions of the CF-structured $MgAl_2O_4$ phase at approximately 40 GPa as phase boundaries of higher-pressure polymorphs are not well constrained. The $Al_2O_3$ solubility in FeO-bearing ferropericlase appears to be almost identical to that of periclase, implying that FeO has little effect. Further thermodynamic calculations in a more representative mantle system (MgO-$SiO_2$-$Al_2O_3$) indicate that, throughout the mantle, the ferropericlase $Al_2O_3$ content cannot exceed 0.5 mol.% under current adiabatic mantle temperatures. Such a small content of $Al_2O_3$ will not influence the thermoelastic properties of ferropericlase, but could still influence transport properties as such concentrations have been reported to affect Mg self-diffusion.

Ferropericlase inclusions in diamonds have $Al_2O_3$ contents that vary up to approximately 0.35 mol. %. If such inclusions could be reliably considered to have formed contemporaneously with other $Al_2O_3$-rich inclusions such as garnets in the same diamond, then the concentration can be used to determine the temperature of formation. However, for most inclusions the $Al_2O_3$ activity at formation will be unknown and our model can only be used to determine the maximum $Al_2O_3$ solubility assuming coexistence with a $Al_2O_3$-rich phase of the mantle. Using this solubility relationship, conditions in the mantle can be excluded at which some ferropericlase inclusions could have formed because their $Al_2O_3$ contents would be too high. Thermodynamic calculations show that the solubility of $Al_2O_3$ in ferropericlase at mantle adiabatic conditions goes through two maxima, at the base of the upper mantle and top of the lower mantle. By comparison, the solubility at transition zones conditions goes through a minimum throughout the garnet stability field. As a result, a few ferropericlase inclusions can be excluded from formation in the transition zone as their $Al_2O_3$ contents are higher than even super adiabatic conditions would produce. These high-$Al_2O_3$ content inclusions must have been formed, however, at temperatures within 100 K of a typical mantle adiabat, either at the base of the upper mantle or at the very top of the lower mantle.

## 6. Data availability

Data are available through Zenodo at https://doi.org/10.5281/zenodo.10828212.

## CRediT authorship contribution statement

**Lianjie Man:** Writing – original draft, Visualization, Methodology, Investigation, Formal analysis, Data curation, Conceptualization. **Hongzhan Fei:** Writing – review & editing, Investigation, Conceptualization. **Eun Jeong Kim:** Writing – review & editing, Investigation. **Adrien Néri:** Writing – review & editing, Investigation. **Longjian Xie:** Writing – review & editing, Investigation. **Daniel J. Frost:** Writing – review & editing, Visualization, Methodology, Funding acquisition, Formal analysis, Conceptualization.

## Declaration of competing interest

The authors declare that they have no known competing financial interests or personal relationships that could have appeared to influence the work reported in this paper.

## Acknowledgments

We thank H. Fischer and S. Übelhack for their technical assistance in the machining of multi-anvil assemblies and maintenance of the presses, and thank R. Njul and A. Rother for their help with sample preparation. We appreciate thoughtful discussions with A. Withers and the constructive comments of three reviewers and the associate editor. This research was supported by DFG grant FR1555/11.

## Appendix A. Supplementary material

This document contains additional figures and tables referred to in the paper. Fig. S1 shows modelling of EPMA secondary fluorescence. Fig. S2 shows X-ray diffraction patterns of CF and CT phases. Fig. S3 is a comparison between the thermodynamic model and the experimental data between 25 and 55 GPa at different temperatures. Fig. S4 is an image of an experimental sample containing ferropericlase and periclase sample. Fig. S5 shows the adiabatic temperature profile used in this study. Tables report the chemical composition of the $Al_2O_3$-rich phases coexisting with periclase (Table S1), and the parameters used for thermodynamic modeling in this study (Tables S2–S4). Supplementary material to this article can be found online at https://doi.org/10.1016/j.gca.2024.05.002.

## References

Akaogi, M., Hamada, Y., Suzuki, T., Kobayashi, M., Okada, M., 1999. High pressure transitions in the system $MgAl_2O_4$–$CaAl_2O_4$: a new hexagonal aluminous phase with implication for the lower mantle. Phys. Earth Planet. In. 115, 67–77.

Alper, A.M., McNally, R.N., Ribbe, P.H., Doman, R.C., 1962. The system MgO–$MgAl_2O_4$. J. Am. Ceram. Soc. 45, 263–268.

Ammann, M.W., Brodholt, J.P., Dobson, D.P., 2012. Diffusion of aluminium in MgO from first principles. Phys. Chem. Miner. 39, 503–514.

Angel, R.J., Alvaro, M., Nestola, F., 2022. Crystallographic methods for non-destructive characterization of mineral inclusions in diamonds. Rev. Mineral. Geochem. 88, 257–305.

Anzolini, C., Nestola, F., Mazzucchelli, M.L., Alvaro, M., Nimis, P., Gianese, A., Morganti, S., Marone, F., Campione, M., Hutchison, M.T., Harris, J.W., 2019. Depth of diamond formation obtained from single periclase inclusions. Geology 219–222.

Brey, G.P., Bulatov, V., Girnis, A., Harris, J.W., Stachel, T., 2004. Ferropericlase—a lower mantle phase in the upper mantle. Lithos 77, 655–663.

Bulatov, V.K., Girnis, A.V., Brey, G.P., Woodland, A.B., Höfer, H.E., 2019. Ferropericlase crystallization under upper mantle conditions. Contrib. Mineral. Petrol. 174, 1–14.

Burnham, A.D., Bulanova, G.P., Smith, C.B., Whitehead, S.C., Kohn, S.C., Gobbo, L., Walter, M.J., 2016. Diamonds from the Machado River alluvial deposit, Rondônia, Brazil, derived from both lithospheric and sublithospheric mantle. Lithos 265, 199–213.

Enomoto, A., Kojitani, H., Akaogi, M., Miura, H., Yusa, H., 2009. High-pressure transitions in $MgAl_2O_4$ and a new high-pressure phase of $Mg_2Al_2O_5$. J. Solid State Chem. 182, 389–395.

Frenkel, A.S., Shmukler, K.M., Sukharevskij, B.Y., Gul'ko, N.V., 1960. On the Mechanism of Dissolution and Precipitation of Spinel in a Periclase Solid Solution. Dokl. Akad. Nauk 130, 1095–1098.

Frost, D.J., Langenhorst, F., 2002. The effect of $Al_2O_3$ on Fe-Mg partitioning between magnesiowüstite and magnesium silicate perovskite. Earth Planet. Sci. Lett. 199, 227–241.

Gu, T., Pamato, M.G., Novella, D., Alvaro, M., Fournelle, J., Brenker, F.E., Wang, W., Nestola, F., 2022. Hydrous peridotitic fragments of Earth's mantle 660 km discontinuity sampled by a diamond. Nat. Geosci. 15, 950–954.

Hallstedt, B., 1992. Thermodynamic assessment of the system MgO–$Al_2O_3$. J. Am. Ceram. Soc. 75, 1497–1507.

Harte, B., 1999. Lower mantle mineral associations in diamonds from Sao Luiz, Brazil. In: Fei, Y., Bertka, C.M., Mysen, B.O. (Eds.), Mantle Petrology: Field Observations and High-pressure Experimentation: A Tribute to Francis R. (Joe), Vol. 6. Geochem Soc. Spec. Publ., pp.125–153.

Hayman, P.C., Kopylova, M.G., Kaminsky, F.V., 2005. Lower mantle diamonds from Rio Soriso (Juina area, Mato Grosso, Brazil). Contrib. Miner. Petrol. 149, 430–445.

Henriksen, A.F., Kingery, W.D., 1979. Effects of strain energy on precipitate morphology in MgO. Ceram. Int. 5, 56–60.

Hidayat, T., Shishin, D., Decterov, S.A., Jak, E., 2017. Experimental study and thermodynamic re-optimization of the FeO-$Fe_2O_3$-$SiO_2$ system. J. Ph. Equilibria Diffus. 38, 477–492.

Holland, T.J.B., Powell, R., 2011. An improved and extended internally consistent thermodynamic dataset for phases of petrological interest, involving a new equation of state for solids. J. Metam. Geol. 29, 333–383.

Huang, R., Ballaran, T.B., McCammon, C.A., Miyajima, N., Dolejš, D., Frost, D.J., 2021. The composition and redox state of bridgmanite in the lower mantle as a function of oxygen fugacity. Geochim. Cosmochim. Acta 303, 110–136.

Hutchison, M.T., 1997. The Constitution of the Deep Transition Zone and Lower Mantle Shown by Diamonds and Their Inclusions. University of Edinburgh. Ph.D. Thesis.

Hutchison, M.T., Nixon, P.H., Harley, S.L., 2004. Corundum inclusions in diamonds—discriminatory criteria and a corundum compositional dataset. Lithos 77, 273–286.

Irifune, T., 1994. Absence of an aluminous phase in the upper part of the Earth's lower mantle. Nature 370, 131–133.

Irifune, T., Fujino, K., Ohtani, E., 1991. A new high-pressure form of $MgAl_2O_4$. Nature 349, 409–411.

Irifune, T., Naka, H., Sanehira, T., Inoue, T., Funakoshi, K., 2002. In situ X-ray observations of phase transitions in $MgAl_2O_4$ spinel to 40 GPa using multianvil apparatus with sintered diamond anvils. Phys. Chem. Miner. 29, 645–654.

Irifune, T., Shinmei, T., McCammon, C.A., Miyajima, N., Rubie, D.C., Frost, D.J., 2010. Iron partitioning and density changes of pyrolite in Earth's lower mantle. Science 327, 193–195.

Irifune, T., Tsuchiya, T., 2007. Mineralogy of the Earth-Phase transitions and mineralogy of the lower mantle. Treatise Geophys. 2, 33–62.

Ishii, T., Shi, L., Huang, R., Tsujino, N., Druzhbin, D., Myhill, R., Li, Y., Wang, L., Yamamoto, T., Miyajima, N., Kawazoe, T., 2016. Generation of pressures over 40 GPa using Kawai-type multi-anvil press with tungsten carbide anvils. Rev. Sci. Instrum. 8, 024501.

Ishii, T., Liu, Z., Katsura, T., 2019. A breakthrough in pressure generation by a Kawai-type multi-anvil apparatus with tungsten carbide anvils. Engineering 5, 434–440.

Ishii, T., Criniti, G., Bykova, E., Dubrovinsky, L., Katsura, T., Arii, H., Kojitani, H., Akaogi, M., 2021. High-pressure syntheses and crystal structure analyses of a new low-density $CaFe_2O_4$-related and $CaTi_2O_4$-type $MgAl_2O_4$ phases. Am. Mineral. 106, 1105–1112.

Ishii, T., Frost, D.J., Kim, E.J., Chanyshev, A., Nishida, K., Wang, B., Ban, R., Xu, J., Liu, J., Su, X., Higo, Y., 2023. Buoyancy of slabs and plumes enhanced by curved post-garnet phase boundary. Nat. Geosci. 16, 828–832.

Ita, J., Cohen, R.E., 1998. Diffusion in MgO at high pressure: Implications for lower mantle rheology. Geophys. Res. Lett. 25, 1095–1098.

Jung, I.H., Decterov, S.A., Pelton, A.D., 2004. Critical thermodynamic evaluation and optimization of the FeO-$Fe_2O_3$-MgO-$SiO_2$ system. Metall. Mater. Trans. B 35, 877–889.

Kaminsky, F., 2012. Mineralogy of the lower mantle: a review of 'super-deep' mineral inclusions in diamond. Earth Sci. Rev. 110, 127–147.

Kaminsky, F.V., Ryabchikov, I.D., McCammon, C.A., Longo, M., Abakumov, A.M., Turner, S., Heidari, H., 2015. Oxidation potential in the Earth's lower mantle as recorded by ferropericlase inclusions in diamond. Earth Planet. Sci. Lett. 417, 49–56.

Kaminsky, F., Zakharchenko, O., Davies, R., Griffin, W., Khachatryan-Blinova, G., Shiryaev, A., 2001. Superdeep diamonds from the Juina area, Mato Grosso state, Brazil. Contrib. Mineral. Petrol. 140, 734–753.

Katsura, T., 2022. A revised adiabatic temperature profile for the mantle. J. Geophys. Res. Solid 127, e2021JB023562.

Keppler, H., Frost, D.J., 2005. Introduction to minerals under extreme conditions. EMU Notes Mineral. 7, 1–30.

Kiseeva, E.S., Korolev, N., Koemets, I., Zedgenizov, D.A., Unitt, R., McCammon, C., Aslandukova, A., Khandarkhaeva, S., Fedotenko, T., Glazyrin, K., Bessas, D., 2022. Subduction-related oxidation of the sublithospheric mantle evidenced by ferropericlase and magnesiowüstite diamond inclusions. Nat. Commun. 13, 7517.

Kohn, M.J., Mazzucchelli, M.L., Alvaro, M., 2023. Elastic thermobarometry. Annu. Rev. Earth Planet. Sci. 51, 331–366.

Kojitani, H., Enomoto, A., Tsukamoto, S., Akaogi, M., Miura, H., Yusa, H., 2010. High-pressure high-temperature phase relations in $MgAl_2O_4$. J. Phys. Conf. Ser. 215, 012098.

Kojitani, H., Ishii, T., Akaogi, M., 2012. Thermodynamic investigation on phase equilibrium boundary between calcium ferrite-type $MgAl_2O_4$ and MgO+ α-$Al_2O_3$. Phys. Earth Planet. Inter. 212, 100–105.

Liu, L.G., 1975. Disproportionation of MgAl2O4 spinel at high pressures and temperatures. Geophys. Res. Lett. 2, 9–11.

Liu, L.G., 1978. A new high-pressure phase of spinel. Earth Planet. Sci. Lett. 41, 398–404.

Liu, L.G., 2002. An alternative interpretation of lower mantle mineral associations in diamonds. Contrib. Miner. Petrol. 144, 16–21.

Liu, Z., Nishi, M., Ishii, T., Fei, H., Miyajima, N., Ballaran, T.B., Ohfuji, H., Sakai, T., Wang, L., Shcheka, S., Arimoto, T., Tange, Y., Higo, Y., Irifune, T., Katsura, T., 2017. Phase relations in the system $MgSiO_3$-$Al_2O_3$ up to 2300 K at lower mantle pressures. J. Geophys. Res. Solid 122, 7775–7788.

Liu, Z., Akaogi, M., Katsura, T., 2019a. Increase of the oxygen vacancy component in bridgmanite with temperature. Earth Planet. Sci. Lett. 505, 141–151.

Liu, Z., Ballaran, T.B., Huang, R., Frost, D.J., Katsura, T., 2019b. Strong correlation of oxygen vacancies in bridgmanite with Mg/Si ratio. Earth Planet. Sci. Lett. 523, 115697.

Llovet, X., Francesc, S., 2017. PENEPMA: a Monte Carlo program for the simulation of X-ray emission in electron probe microanalysis. Microsc. Microanal. 23, 634–646.

Lorenzon, S., Wenz, M., Nimis, P., Jacobsen, S.D., Pasqualetto, L., Pamato, M.G., Novella, D., Zhang, D., Anzolini, C., Regier, M., Stachel, T., 2023. Dual origin of ferropericlase inclusions within super-deep diamonds. Earth Planet. Sci. Lett. 608, 118081.

Luth, R.W., Virgo, D., Boyd, F.R., Wood, B.J., 1990. Ferric iron in mantle-derived garnets: Implications for thermobarometry and for the oxidation state of the mantle. Contrib. to Mineral. Petrol. 104, 56–72.

McCammon, C., Hutchison, M., Harris, J., 1997. Ferric iron content of mineral inclusions in diamonds from Sao Luiz: a view into the lower mantle. Science 278, 434–436.

McCammon, C.A., Stachel, T., Harris, J.W., 2004. Iron oxidation state in lower mantle mineral assemblages: II. Inclusions in diamonds from Kankan, Guinea. Earth Planet. Sci. Lett. 222, 423–434.
Mori, T., 1982. Solubility of $Al_2O_3$ in MgO. Yogyo-Kyokai-Shi 90, 551–552.
Nestola, F., Pamato, M.G., Novella, D., Wang, Y., Qu, K., Smith, E.M., 2023a. Elastic geobarometry yielding a faithful sublithospheric depth for a ferropericlase inclusion in diamond. Lithos 454–455, 107265.
Nestola, F., Regier, M.E., Luth, R.W., Pearson, D.G., Stachel, T., McCammon, C., Wenz, M.D., Jacobsen, S.D., Anzolini, C., Bindi, L., Harris, J.W., 2023b. Extreme redox variations in a superdeep diamond from a subducted slab. Nature 613, 85–89.
Nestola, F., Prencipe, M., Belmonte, D., 2023c. $Mg_3Al_2Si_3O_{12}$ jeffbenite inclusion in super-deep diamonds is thermodynamically stable at very shallow Earth's depths. Sci. Rep. 13, 83.
Nimis, P., 2022. Pressure and temperature data for diamonds. Rev. Mineral. Geochem. 88, 533–565.
Nimis, P., Nestola, F., Schiazza, M., Reali, R., Agrosì, G., Mele, D., Tempesta, G., Howell, D., Hutchison, M.T., Spiess, R., 2019. Fe-rich ferropericlase and magnesiowüstite inclusions reflecting diamond formation rather than ambient mantle. Geology 47, 27–30.
Nishihara, Y., Doi, S., Kakizawa, S., Higo, Y., Tange, Y., 2020. Effect of pressure on temperature measurements using WRe thermocouple and its geophysical impact. Phys. Earth Planet. In. 298, 106348.
O'Neill, H.S.C., Wall, V.J., 1987. The Olivine-Orthopyroxene-Spinel oxygen geobarometer, the nickel precipitation curve, and the oxygen fugacity of the Earth's Upper Mantle. J. Petrol. 28, 1169–1191.
Ono, S., Ohishi, Y., Isshiki, M., Watanuki, T., 2005. In situ X-ray observations of phase assemblages in peridotite and basalt compositions at lower mantle conditions: implications for density of subducted oceanic plate. J. Geophys. Res. Solid 110, B02208.
Ono, S., Kikegawa, T., Ohishi, Y., 2006. The stability and compressibility of $MgAl_2O_4$ high-pressure polymorphs. Phys. Chem. Miner. 33, 200–206.
Riet, A.A., Van Orman, J.A., Lacks, D.J., 2020. Molecular dynamics simulation of vacancy-solute binding free energy in periclase. Phys. Chem. Miner. 47, 38.
Seitz, H.M., Brey, G.P., Harris, J.W., Durali-Müller, S., Ludwig, T., Höfer, H.E., 2018. Ferropericlase inclusions in ultradeep diamonds from Sao Luiz (Brazil): high Li abundances and diverse Li-isotope and trace element compositions suggest an origin from a subduction mélange. Mineral. Petrol. 112, 291–300.
Sempolinski, D.R., Kingery, W.D., 1980. Ionic conductivity and magnesium vacancy mobility in magnesium oxide. J. Am. Ceram. Soc. 63, 664–669.
Stachel, T., 2001. Diamonds from the asthenosphere and the transition zone. Eur. J. Mineral. 13, 883–892.
Stixrude, L., Lithgow-Bertelloni, C., 2022. Thermal expansivity, heat capacity and bulk modulus of the mantle. Geophys. J. Int. 228, 1119–1149.
Stubican, V.S., Roy, R., 1965. Mechanism of the precipitation of the spinel from MgO-$Al_2O_3$ solid solutions. J. Phys. Chem. Solid 26, 1293–1297.
Thomson, A.R., Walter, M.J., Kohn, S.C., Brooker, R.A., 2016. Slab melting as a barrier to deep carbon subduction. Nature 529, 76–79.
Van Orman, J.A., Fei, Y., Hauri, E.H., Wang, J., 2003. Diffusion in MgO at high pressures: Constraints on deformation mechanisms and chemical transport at the core-mantle boundary. Geophys. Res. Lett. 30, 1056.
Van Orman, J.A., Li, C., Crispin, K.L., 2009. Aluminum diffusion and Al-vacancy association in periclase. Phys. Earth Planet. In. 172, 34–42.
van Westrenen, W., van Orman, J.A., Watson, H., Fei, Y., Watson, E.B., 2003. Assessment of temperature gradients in multianvil assemblies using spinel layer growth kinetics. Geochem. Geophys. Geosyst. 4, 474.
Walter, M.J., Kohn, S.C., Araujo, D., Bulanova, G.P., Smith, C.B., Gaillou, E., Wang, J., Steele, A., Shirey, S.B., 2011. Deep mantle cycling of oceanic crust: evidence from diamonds and their mineral inclusions. Science 334, 54–57.
Walter, M.J., Thomson, A.R., Smith, E.M., 2022. Geochemistry of silicate and oxide inclusions in sublithospheric diamonds. Rev. Mineral. Geochem. 88, 393–450.
Whitney II, W.P., Stubican, V.S., 1971. Interdiffusion studies in the system MgO-$Al_2O_3$. J. Phys. Chem. Solid 32, 305–312.
Wirth, R., Dobrzhinetskaya, L., Harte, B., Schreiber, A., Green, H.W., 2014. High-Fe (Mg, Fe) O inclusion in diamond apparently from the lowermost mantle. Earth Planet. Sci. Lett. 404, 365–375.
Zienert, T., Fabrichnaya, O., 2013. Thermodynamic assessment and experiments in the system MgO–$Al_2O_3$. Calphad 40, 1–9.